UNIVERSITÉ DE MONTRÉAL

SOLID DISPERSION IN A VISCOUS NEWTONIAN PHASE USING A DUAL SHAFT MIXER

SANAZ AGHA BARAR POUR TABBAKHI

DÉPARTEMENT DE GÉNIE CHIMIQUE

ÉCOLE POLYTECHNIQUE DE MONTRÉAL

MÉMOIRE PRÉSENTÉ EN VUE DE L'OBTENTION

DU DIPLÔME DE MAÎTRISE ÈS SCIENCES APPLIQUÉES

(GÉNIE CHIMIQUE)

OCTOBRE 2006

© SANAZ BARAR POUR TABBAKHI, 2006

Library and Archives Canada

Published Heritage Branch

395 Wellington Street
Ottawa ON K1A 0N4
Canada

Bibliothèque et Archives Canada

Direction du Patrimoine de l'édition

395, rue Wellington
Ottawa ON K1A 0N4
Canada

Your file Votre référence
ISBN: 978-0-494-25524-7
Our file Notre référence
ISBN: 978-0-494-25524-7

NOTICE:
The author has granted a non-exclusive license allowing Library and Archives Canada to reproduce, publish, archive, preserve, conserve, communicate to the public by telecommunication or on the Internet, loan, distribute and sell theses worldwide, for commercial or non-commercial purposes, in microform, paper, electronic and/or any other formats.

The author retains copyright ownership and moral rights in this thesis. Neither the thesis nor substantial extracts from it may be printed or otherwise reproduced without the author's permission.

AVIS:
L'auteur a accordé une licence non exclusive permettant à la Bibliothèque et Archives Canada de reproduire, publier, archiver, sauvegarder, conserver, transmettre au public par télécommunication ou par l'Internet, prêter, distribuer et vendre des thèses partout dans le monde, à des fins commerciales ou autres, sur support microforme, papier, électronique et/ou autres formats.

L'auteur conserve la propriété du droit d'auteur et des droits moraux qui protège cette thèse. Ni la thèse ni des extraits substantiels de celle-ci ne doivent être imprimés ou autrement reproduits sans son autorisation.

In compliance with the Canadian Privacy Act some supporting forms may have been removed from this thesis.

While these forms may be included in the document page count, their removal does not represent any loss of content from the thesis.

Conformément à la loi canadienne sur la protection de la vie privée, quelques formulaires secondaires ont été enlevés de cette thèse.

Bien que ces formulaires aient inclus dans la pagination, il n'y aura aucun contenu manquant.

Canada

UNIVERSITE DE MONTREAL

ÉCOLE POLYTECHNIQUE DE MONTRÉAL

Ce mémoire intitulé:

SOLID DISPERSION IN A VISCOUS NEWTONIAN PHASE USING A DUAL SHAFT MIXER

présenté par: AGHA BARAR POUR TABBAKHI, Sanaz

en vue de l'obtention du diplôme de: Maîtrise ès sciences appliquées

a été dûment accepté par le jury d'examen constitué de:

M. JOLICOEUR, Mario, Ph.D., président

M. TANGUY Philippe A., Ph.D., membre et directeur de recherche

M. LEGROS Robert, Ph.D., membre

To My Parents

ACKNOWLEDGMENTS

First of all, I would like to thank my supervisor, Professor Philippe Tanguy for accepting me in his research group, for his confidence in my abilities and for his encouragements during my work which made difficulties much easier during the last two years. I would also like to thank him for his financial support.

I am also extremely grateful to Dr. Louis Fradette for his help, kindness and his great availability during my project. I would like to thank Dr. Alfa Arzate for her great support in the first year of my study.

I would like to thank everyone in URPEI research group; Dr. Avinash Khopkar and Francois Cabaret and my colleagues for their great attitude.

I would like to thank my parents, and my brother for their patience, unconditional love, encouragements and financial support. This work was not possible without their presence.

RÉSUMÉ

Le but de ce travail était de caractériser expérimentalement l'hydrodynamique d'un mélangeur à deux arbres d'agitation (dual). Le mélangeur étudié est composé d'un agitateur dispersant (Deflo) et d'un mobile raclant (Paravisc), ces deux agitateurs étant montés sur deux arbres de rotation différents. L'agitateur dispersant, tournant à haute vitesse, est positionné sur un arbre excentré tandis que le mobile raclant, qui lui tourne à faible vitesse, est placé sur un arbre centré. L'indépendance des deux arbres de rotation permet de faire tourner les deux mobiles à des vitesses différentes, ainsi différents rapports de vitesses entre les deux agitateurs ($N_{Deflo}/N_{Paravisc}$) peuvent être choisis. Cette liberté de rotation des deux agitateurs nous permet à la fois de mélanger un liquide Newtonien visqueux et de disperser un solide dans ce même liquide. Dans ce travail, il est proposé de caractériser la consommation de puissance et l'efficacité du mélange afin d'améliorer la connaissance sur ce mélangeur, quantifier ses performances et d'avoir une base pour effectuer sa mise à l'échelle.

Bien que le mélangeur à deux arbres de rotation présente une cinématique de mélange complexe, l'interaction entre les deux agitateurs a été caractérisée. Il a été démontré que la vitesse de rotation d'une turbine Deflo a une grande influence sur la consommation de puissance du Paravisc. Lorsque la vitesse de rotation de la Deflo augmente, la consommation de puissance du Paravisc diminue. Cependant, le Paravisc n'a montré aucune influence sur la consommation de puissance de la Deflo. Les temps de mélange ont été déterminés à différents ratios de vitesse et à différentes viscosités. Ceux-ci ont été déterminés par analyse d'images en utilisant le logiciel IMAGE PRO-PLUS. Nous avons montré que le procédé de mélange est principalement gouverné par le Paravisc; cependant, la Deflo montre une grande capacité de pompage, principalement à basse viscosité. La consommation de puissance et les mesures de taille de particules ont été réalisées pour la dispersion solide-liquide. Le liquide utilisé était un fluide newtonien visqueux et les solides étaient du carbonate de calcium et des billes de verre à une

concentration de 10% en masse. L'étude de la consommation de puissance des agitateurs a montré l'influence de la vitesse de rotation des agitateurs sur le temps de dispersion. Il a été trouvé que la turbine Deflo (mobile dispersant) avait une grande efficacité pour casser les flocs et les agglomérats présents dans la cuve de mélange.

ABSTRACT

The goal of this work is to characterize in an experimental way the hydrodynamics of a dual-shaft mixer. This mixer is composed of a dispersing impeller and a Paravisc impeller mounted on two independent shafts. The dispersing turbine is located in an off-centered position rotating at high speed, while the other shaft rotating at low speed supports the wall-scraping Paravisc. The independence of each agitator drive makes it possible to operate the system at the desired rotational speed ratio; that is the rotational speed of the Deflo over the rotational speed of the Paravisc ($N_{Deflo}/N_{Paravisc}$). This autonomy allows us to verify the homogenization of high viscosity Newtonian fluids and solid-liquid dispersion. In this work, it is proposed to characterize the power consumption and mixing efficiency in single phase and two phase flow in order to improve the knowledge about device performance and provide a scientifically-based design for scale up.

Although the dual-shaft mixer follows complex kinematics, it was possible to study the interaction between the impellers. It was demonstrated that, the Deflo rotational speed has great influence on the Paravisc power consumption. As the rotational speed of the Deflo increases, the power dissipated by the Paravisc decreases. However, no influence of the Paravisc was observed on the Deflo power consumption. Mixing times were measured using the IMAGE PRO-PLUS technique at various combinations of rotational speed ratios in different viscosities. It was found that the mixing process is mainly governed by the Paravisc; however, the Deflo shows a great pumping capacity especially at lower viscosities.

Power consumption and particle size measurements were carried out with a high viscosity solid-liquid dispersion of calcium carbonate and glass beads at 10 wt% solids concentration. Studying of the impellers power consumption showed the influence of impeller rotational speed on dispersion time. It was found that the Deflo disperser has a

great ability to break up lumps and agglomerates within the vessel resulting in a homogenous dispersion.

CONDENSÉ EN FRANÇAIS

Le mélange solide-liquide à grande viscosité est une opération de mélange très commune dans les industries suivantes :

- Cosmétique
- Pâtes et papier
- Alimentaire
- Enduits et de peintures
- Traitement de polymères
- Etc.

Dans ces applications, l'obtention d'un mélange homogène est difficile à obtenir, car il n'y pas beaucoup de mouvement et de turbulence dans la cuve afin de bien distribuer les différents composants. La viscosité du mélange amène beaucoup de dissipations visqueuses dans la cuve, ce qui provoque des augmentations significatives de la température. Pour des fluides de basse viscosité, les systèmes de mélange les plus communs sont basés sur des turbines à pale droite qui tournent à grande vitesse. En présence d'un fluide visqueux, ces turbines perdent leur efficacité en raison du grand dégagement de chaleur autour de la turbine, ce qui créé des zones mortes et des effets de caverne. Afin d'écarter ce problème, il est possible d'utiliser des mélangeurs raclants tels que le ruban hélicoïdal, l'ancre ou le Paravisc tournant à vitesse réduite. Ces agitateurs fournissent un écoulement axial plus efficace. Une bonne homogénéisation dans ces systèmes serait ainsi réalisée. Habituellement, dans un mélange biphasique, par exemple un mélange solide-liquide, où la phase continue est visqueuse, deux mécanismes sont nécessaires pour effectuer le mélange : tout d'abord, la diminution de la taille des agrégats de particules, et, en second lieu, l'obtention d'un haut degré d'uniformité dans la cuve. La combinaison des agitateurs mentionnés ci-dessus peut aider à relever ce défi. Dans une application simple où le grand degré de polyvalence

n'est pas exigé, les mélangeurs à deux arbres de rotation sont satisfaisants pour obtenir une bonne qualité de produit. Dans ces mélangeurs, deux types d'agitateurs sont typiquement employés:

- Agitateur raclant tournant à vitesse réduite;
- Disperseur tournant à grande vitesse et fournissant un haut cisaillement .

Dans cette étude, un agitateur Paravisc est employé comme agitateur de proximité. Cet agitateur induit un faible cisaillement, favorisant un mélange doux tout en générant l'écoulement latéral et transversal requis pour le mélange. Le disperseur à grande vitesse est une turbine Deflo située en position décentrée. Elle permet de fournir le cisaillement élevé requis pour la dispersion et contribue positivement au pompage du fluide. Une turbine Deflo se compose d'un disque bordé par des dents légèrement obliques, alternativement positionnées en haut et en bas du disque. Ce disperseur permet d'obtenir une bonne dispersion de suspensions fortement pigmentées. À notre connaissance, aucune étude n'est disponible pour un tel système de mélange où sont associés un agitateur centré principal et une turbine de dispersion décentrée, bien que ce type de mélangeur jouisse d'une utilisation répandue dans l'industrie. L'objectif principal de cette étude est donc de fournir une base scientifique à la performance de ce mélangeur dual en présence d'une phase continue newtonienne visqueuse, mais aussi lors de son utilisation pour la dispersion solide-liquide, elle aussi en milieu visqueux. Les objectifs spécifiques sont de :

- Clarifier la consommation de puissance et déterminer le temps de mélange avec des phases continues visqueuses.
- Clarifier la consommation de puissance lors de la dispersion solide-liquide et déterminer le temps de dispersion afin d'établir l'efficacité d'homogénéisation du mélangeur.

Dans les expériences réalisées, des solutions glucose-eau ont été employées comme fluide newtonien en phase continue. Ce type de fluide est transparent et la gamme de la viscosité varie de 1 à 11 Pa.s. Les phases solides étaient formées de carbonate de calcium et de billes de verre. La concentration en solide était toujours de 10% en masse lors des différentes expériences. Les mesures de temps de mélange ont été faites par analyse d'images d'une décoloration obtenue par une réaction acide-base. Pour étudier l'efficacité d'homogénéisation, des échantillons de la dispersion ont été prélevés près de la surface de la cuve et la distribution de taille des échantillons a été déterminée à l'aide d'un granulomètre de type Mastersizer « S ».

Les expériences ont montré que l'augmentation de la vitesse de rotation de la turbine Deflo abaisse la consommation de puissance du Paravisc. À l'opposé, le Paravisc ne présentait aucun effet sur la Deflo. Il a été constaté que la turbine Deflo offre une bonne capacité de pompage indépendamment de la viscosité de la phase continue. Des mesures de puissance et de temps de mélange ont permis de déterminer que les meilleures conditions de mélange sont atteintes lorsque la puissance est également répartie entre les agitateurs. Bien que le Paravisc régisse le processus de mélange global, il devrait toujours fonctionner avec une chicane ou en combinaison avec un autre agitateur pouvant en tenir lieu. L'efficacité d'homogénéisation d'une dispersion a été aussi investiguée. Une crête dans la consommation de puissance de la Deflo et un minimum dans celle du Paravisc ont pu être expliqués par la possibilité de formation d'agglomérats. Cette hypothèse a été validée avec des mesures de distribution de tailles des solides. Ces mesures ont montré la capacité de la réduction de taille de la turbine Deflo. Les mesures de puissance ont aussi confirmé l'influence du Paravisc sur l'obtention d'une taille minimum de la phase dispersée en raison du pompage qui ramène le solide dans la zone de dispersion de façon efficace.

TABLE OF CONTENTS

LIST OF TABLES

LIST OF FIGURES

LIST OF SYMBOLS AND ABBREVIATIONS

Roman Characters

Symbol	Description	Unite
a	Characteristic length of the particle	(-)
a	Coefficient	(-)
A	Hamaker constant	(-)
A	Calibration factor	(-)
C_D	Drag coefficient	(-)
C_{Deflo}	Deflo clearance	(m)
$C_{Paravisc}$	Paravisc clearance	(m)
d_p	Particle size	(m)
D	Impeller diameter	(m)
D_{Deflo}	Deflo diameter	(m)
$D_{paravisc}$	Paravisc diameter	(m)
D_a	Anchor diameter	(m)
D_t	Turbine diameter	(m)
E	Extinction coefficient	(-)
Fr	Froude number	(-)
g	Acceleration of gravity	(m/s^2)
I	Light after absorption	(-)
I_0	Intensity of the incident light	(-)
k	Boltzmann's constant	(-)
k	Parameter of structure	(-)
K_P	Power constant	(-)

$K_P(n)$	Power constant (for non-Newtonian fluids)	(-)
K_{Pancre}	Anchor power constant	(-)
$K_{rods+PBT}$	Rods and PBT power constant	(-)
K_s	Shear rate constant	(-)
m	Flow consistency index	($Pa.s^n$)
M_c	Corrected torque	(N-m)
M_m	Measured torque	(N-m)
M_r	Residual torque	(N-m)
n	Rotational frequency	(1/s)
n	Power law index	(-)
N'	Dual shaft rotational speed	(rps)
N	Impeller rotational speed	(rps)
N_a	Anchor rotational speed	(rps)
N_t	Turbine rotational speed	(rps)
N_{Deflo}	Deflo rotational speed	(rps)
N_{js}	Impeller speed for just suspended	(rps)
$N_{Paravisc}$	Paravisc rotational speed	(rps)
N_P	Power number	(-)
N_P *	Modified power number	(-)
P	Power consumption	(W)
P_{Deflo}	Deflo power consumption	(W)
$P_{paravisc}$	Paravisc power consumption	(W)
P_{NN}	Power consumption on non-Newtonian fluid	(W)
P_N	Power consumption in Newtonian fluid	(W)
P_{tot}	Total power consumption	(W)

Re	Reynolds number	(-)
Re_{pl}	Power law Reynolds number	(-)
Re_{imp}	Impeller Reynolds number	(-)
Re_g	Generalized Reynolds number	(-)
Re*	Modified Reynolds number	(-)
R_N	Rotational speed ratio	(-)
S	Zwietering constant	(-)
T	Absolute temperature	(°K)
T	Tank diameter	(m)
T_m	Mixing time	(s)
U	Particle velocity	(m/s)
V_t	Settling velocity	(m/s)
V_{ts}	Hindered velocity	(m/s)
X	Mass ratio of suspended solids to liquid	
Greek Characters		
α	Exponent	(-)
β	Exponent	(-)
ρ	Fluid density	(kg/m^3)
ρ_l	Liquid density	(kg/m^3)
ρ_s	Solid density	(kg/m^3)
ρ^*	Suspension density	(kg/m^3)
μ	Fluid viscosity	(Pa.s)
μ_o	Viscosity of continuous phase	(Pa.s)
μ_r	Relative viscosity	(-)
μ_{eff}	Effective viscosity	(Pa.s)

μ^*	Suspension viscosity	(Pa.s)
η_a	Apparent viscosity of non-Newtonian fluid	(Pa.s)
ψ	Particle shape or sphericity	(-)
θ	Dimensionless mixing time	(-)
ε	Dielectric constant	(-)
ε_0	Permittivity of vacuum	($F.m^{-1}$)
ε_S	Volume fraction of solids	(%w/w)
ψ_S	Surface potential	(-)
γ	Surface tension	($N.m^{-1}$)
$\dot{\gamma}_e$	Effective shear rate	(s^{-1})
ϕ	Rotational frequency ratio	(-)
ϕ	Volume fraction of solids in suspension	(% w/w)
ϕ_m	Maximum volume fraction of particles	(% w/w)
φ_M	Packing concentration	(% w/w)
ϕ_v	Solid volume concentration	(% w/w)
υ	Kinematic viscosity of the liquid	($m^2.s^{-1}$)
κ	Measured conductivity	(koh m^{-1})
κ_O	Conductivity in the absence of solids	(koh m^{-1})
κ_C	Corrected conductivity	(koh m^{-1})
κ_M	Measured conductivity	(koh m^{-1})
κ_{OR}	Fluid conductivity at the reference temperature	(koh m^{-1})
κ_{OM}	Fluid conductivity	(koh m^{-1})
ℓ	Optical path length	(m)

Chapter 1 - Introduction

1.1 Importance of mixing in process industries

Mixing plays a key role in processing operation. Heat and mass transfer are greatly influenced by mixing. There is no doubt that mixing is a central feature in chemical process industries such as:

- Coating , inks , paints
- Polymer processing
- Drinking water and waste water treatment
- Pharmaceutical
- Cosmetic
- Pulp and paper
- Mineral processing
- Petrochemical
- Biotechnology

In 1989 in the USA, the estimated cost to the processing industry due to poor mixing was between $1 and $10 billion in the chemical sector alone (Paul et al., 2004). In comparison with other chemical engineering processes which are developed theoretically, the "art" of mixing has considerable effect on economics, environmental protection, human health, etc.

Generally, in mixing, one has to deal with at least two phases of material. In table 1-1 a classification of mixing application is given. In this table it can be seen that physical processing and chemical processing are associated with each application class. However in many processes such as liquid-solid-gas or liquid-liquid-solid-gas more than one application class is involved.

Table 1-1 Mixing process (Oldshue et al., 1990)

Physical processing	Application class	Chemical processing
Suspension	Liquid-Solid	Dissolving
Dispersion	Liquid-Gas	Absorption
Emulsification	Immiscible Liquids	Extraction
Blending	Miscible Liquids	Reactions
Pumping	Fluid Motion	Heat Transfer

The previous table shows the different mixing application classes. The suspension of particulate solids in a continuous liquid phase is defined as a suspension. Chemical engineers very often have to deal with mechanically agitated solid – liquid suspensions. Suspensions of solid particles in agitated vessels are required in many industrial units such as catalytic reactions, crystallization, leaching, polymerization, dissolution, ion-exchange, and adsorption.

The major objective of solid – liquid mixing is to create and maintain a homogenous slurry or to improve the rate of mass and heat transfer between the solid and liquid phases.

1.1.1 Solid-Liquid Mixing

Solid – liquid mixing is employed in a wide range of industrial applications such as:

- Simple suspension

  Here the aim is to obtain a uniform insoluble solid slurry in a liquid medium. Other applications like adsorption (ion-exchange resin in solution) or resuspension after decantation (washing of crystals or precipitates such as cellulose acetate) fall into this category.

- Particle reduction

Generally the slurry process can be separated in two independent unit operations: pigment wetting and size reduction of agglomerates (Makinen and Nordstorm, 1993). Shear forces greater than those present in suspension are used to reduce the particle size of the agglomerates. Examples are repulping of filter cake and fiberizing wood-pulp stock.

- Dissolution or leaching

Suspension may be applied to obtain dissolution of a soluble or partially soluble solid in liquid.

- Reaction

In more complicated mixing problems, chemical reactions are involved. Some examples include dissolving lead in caustic to make sodium plumbite or suspending a solid catalyst in a reaction mixture.

- Solid formation

In a liquid mixture when a solid is produced, moderate shear forces may be needed in order to control the particle size. Production of rubber curd from latex is an example of this operation.

Each year, in industrial processes there is a gradual increase in formulations that involve higher viscosities. On the process line, products must be of higher quality and experience faster mix cycles. To reach this goal multi-shaft mixers enable the operation of two or three different agitators in an endless variety of functional combinations while charging ingredients, mixing and then discharging the final products. The advantage of these agitators is that each of them can be controlled independently and each one is powered by an electronic variable-speed drive (Cohen and Langhorn, 2004).

1.2 Multi-shaft mixers

Mixing in relatively high viscosity liquids (>10 Pa.s) is involved in many industrial applications like manufacturing pastes, putties, chewing gum, soap and grease. (Paul et

al., 2004). In these industrial processes, obtaining a uniform mixture is a difficult task, because there are no turbulent eddies to help distribute components. In addition most high viscosity fluids are non-Newtonian. The viscous energy dissipation during mixing may lead to significant temperature variation through the vessel. Heat transfer coefficients are low in viscous systems and the methods of increasing heat transfer are counterproductive because of the heat produced from viscous energy dissipation.
Because the diffusion coefficients are extremely low due to the high matrix viscosity, in mixers which handle viscous products it is necessary to promote both lateral and transverse motion. Multi-shaft mixers can be used to carry out this task. These mixers are used in batch processing and are usually found to increase productivity and process versatility (Cohen and Langhorn, 2004) In general, multiple-shaft mixers are capable of integrating several mixing steps in one vessel; a quality which could make many specialized pieces of equipment obsolete. Furthermore, having separate mixing shafts makes maintenance easier than on a concentric shaft mixer.

1.3 Dual-shaft mixers

In simple applications where utmost versatility is not required, using dual-shaft mixers will suffice. In dual-shaft mixers two types of impellers are typically used:

- Low speed shaft impeller
- High speed shaft impeller

- The low speed impeller is a center mounted impeller. In Figure 1-1 an anchor impeller is illustrated. The basic anchor structure includes three horizontal arms and vertical flights. Running at a top speed of 25 to 525 rpm, it feeds the high speed impeller by blending or folding the vessel content and improves the product uniformity by scrapping the walls (Cohen and Langhorn, 2004). By stimulating mass flow, the anchor helps to disperse the heat within the tank. The nonstick scrapers mounted on the impeller prevent segregated layers from

accumulating on the inner surface of the tank. They remove stagnant material and push it towards the inside of the tank. In applications that requires top to bottom flow, (for example to distribute the solid particles through the tank in order to increase homogeneity) the Paravisc can be used to promote axial flow and prevent stratification. (Figure 1-2)

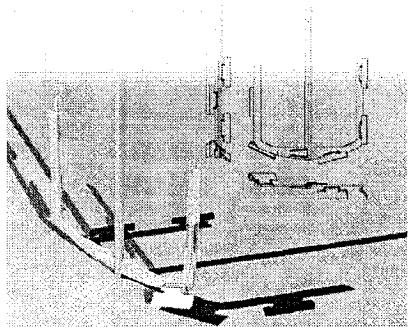

Figure 1-1 Anchor

Figure 1-2 Paravisc (Ekato)

- The high speed impeller provides high shear to disperse or dissolve the dispersed phase, producing substantial flow and a vortex both above and below the blade. It can be configured with many different blade styles (Figure 1-3). One of the advantages of this agitator is that it can reduce and disperse the solid particles that are too large for rotor-stator (Cohen and Langhorn, 2004). However, creating a vortex below and above the blade pulls the material from both the top and bottom of the tank into the high shear zone, which may cause serious

problems such as the incorporation of air into the batch, necessitating a deaeration phase.

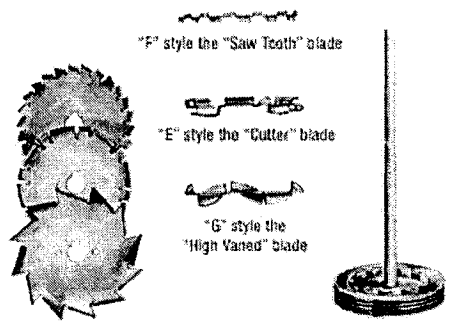

Figure 1-3 High speed dispersers

Although high shear agitators can handle many mixing tasks, hot spots are created near these agitators which can degrade many materials. In order to avoid thermal damage and stratification, a high flow of materials throughout the mixing tank is required, promoting top-to-bottom flow. Here, the Paravisc is a great tool that increases the homogeneity of the mixture and enables the high shear disperser to perform mixing tasks at fluid viscosities of up to 500 Pa.s. In Figure 1-3 three types of common high shear disperser are shown. The F style (Sawtooth) is the standard used for most dispersing applications, since it produces high shear dispersion, pumping action, and size reduction especially for heavy agglomerates. It is often used in processing paints, inks, slurries and coatings. The E style (cutter blade) is a combination of F and G style blades and offers intense turbulent flow with some shear, especially when used on high vehicle viscosity and high solid solutions, resulting in good dispersion with a high pump rate. This style is favored in dissolving resins. The G style, high vane blade, generates a high pumping action which tends to mix the entire batch efficiently, resulting in high speed blending with low shear, but with excellent flow and circulation. It is used in heavy bodied mixes that require higher shear as obtained from paddle agitation.

1.3.1 Industrial applications

There are many industrial applications using dual-shaft mixers. Companies such as Hockmeyer Equipment Corporation, Dantco Mixer Corporation and Reynolds Industries provide multi-shaft and dual-shaft agitators for applications such as paste inks, coatings, plastisols, adhesives, caulking compounds, and specialty chemicals. In Figure 1-4 two configurations of dual-shaft mixer are presented. These mixers consist of a wall-scraping atypical helical ribbon impeller (Paravisc) which rotates at low speed; and a high speed dispersing turbine (often called "Cowles" turbine) which has the task destroying the solid lumps and distributing the particles within the vessel. Suppliers offer these units as laboratory models, tank-mounted production models and post-mounted versions with fixed or variable speeds, with mechanical drives or variable-frequency drives. Models range from laboratory sizes to pilot line sizes to production sizes with tank capacities exceeding 3000 gallons.

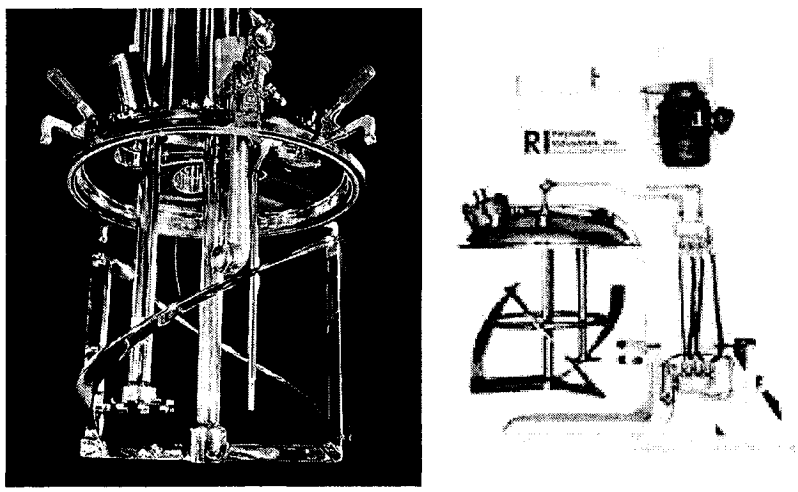

Figure 1-4 Dual-shaft agitator (a) Hockmeyer Equipment incorporation (b) Reynolds industries

1.4 Motivation

For low-viscosity fluids the most common mixing systems are based on high-speed blade turbines such as flat-blade turbine, pitched-blade turbine and hydrofoils in baffled vessels. The study of power draw, discharge characteristics and operating speed is relatively broad. In high-viscosity fluids these turbines lose their efficiency because of the high clearance, dead zones and cavern effects. In order to alleviate these problems, close-clearance impellers such as helical ribbon, anchor, or Paravisc rotating at low speeds could be used. These impellers provide more efficient top-to-bottom flow, and thus good homogenization. In two-phase mixing, for example in solid-liquid mixing of high viscosity continuous phases, usually two mechanisms are required: the first is used to reduce particle size distribution and the second to reach a uniform degree of dispersion homogeneity throughout the vessel. A combination of the impellers mentioned above can achieve this task, resulting in the integration of several mixing step within one vessel. In practice, the following mixing systems are found in industry (Tanguy et al., 1997):

- Multiple intermeshing kneading paddles mounted on a carousel (planetary mixer).
- A main centered impeller associated with off-centered ancillary turbines located close to the vessel surface.
- Co-axial impellers of a similar type rotating at the same speed.
- Co-axial or contra-rotating coaxial impellers with different speeds.

The existence of a scientific basis behind the development of these types of mixing systems is rare, as they have been developed by empirical consideration and industrial experiences. A limited numbers of studies have focused on the mixing performance of planetary mixers (Tanguy et al., 1999, Espinosa-Solares et al. 1997, Zhou et al., 2000) and different types of co-axial mixers (Tanguy et al. 1997, Thibault and Tanguy 2002,

Foucault et al., 2004). However, no studies of a mixing system with a main centered impeller associated with an off-center dispersing turbine exist, despite the widespread industrial use of this type of mixer and its ability to handle mixing tasks in high viscosity mediums.

1.5 General Objective

Based on the previous information and the lack of scientific knowledge pertaining to dual-shaft mixer performance, the main objective of this study is to provide a fundamental and scientifically based explanation of dual-shaft mixing in high viscosity Newtonian continuous phases and highly viscous solid-liquid dispersion. It is proposed to characterize the hydrodynamics of a dual-shaft mixer equipped with a low speed atypical helical ribbon impeller (Paravisc) and an offset high speed disperser in a highly viscous continuous phase and solid-liquid dispersion. Using power consumption characterization, the interaction between the two impellers and their influence on the total mixing process will be explained.

Chapter 2 - Literature Review

Before choosing the mixing system for a particular task, the first step is to increase our knowledge of the product's properties and its rheological behavior. This chapter contains the results of scientific research on this subject and also introduces the appropriate criteria for selecting the appropriate mixing system.

2.1 Solid-liquid systems

Dispersion generally consists of discrete particles randomly distributed in a fluid medium. Dispersion can be divided into three categories: solid particles in a liquid medium (suspension), liquid droplets in a liquid medium (emulsion) or gas bubbles in a liquid (foam). A suspension is a dispersion of particulate solids in a continuous liquid phase which is sufficiently fluid to lend itself to circulation by a mixing device (UHL and Gray, 1967). However, the systems which associate with incorporating powders and fine particles throughout the liquid medium shall be considered as dispersions or colloidal suspensions. (Harnby et al., 1980)

2.1.1 Physical-chemistry properties

The physical and chemical properties of liquid and solid particles influence the fluid-particle hydrodynamics and consequently the suspension. For example, large and dense solids are more difficult to suspend than small particles with low density in the same continued phase. Another example is spherical particles which are more difficult to suspend than thin flat disks (Paul et al., 2004). The properties and operating parameters of solids and suspending fluids are:

a) physical properties of the continuous phase :
   - Liquid density, ρ_l (kg/m³)
   - Density difference, $\rho_s - \rho_l$ (kg/m³)
   - Liquid viscosity, μ_l (Pa.s)

b) physical properties of solid particles :

- Solid density, ρ_s (kg/m³)
- Particle size, d_p (m)
- Particle shape or sphericity, ψ
- Wetting characteristics of the solid
- Tendency to entrap air or head space gas
- Agglomerating tendencies of the solid
- Hardness and friability characteristics of the solid

2.1.2 Force acting on solid particles

A colloidal system is a dispersion of small solid particles in a continuous phase. In this system the ratio of surface area to volume of the solid particles is very high and the particles diameter size varies from 10^{-9} m to 10^{-5} m (Masliyah, 1994). In colloidal suspensions (dispersion) characterized by small particles, forces within a small radius called colloidal forces exist; as the volume concentration of these particles increases, the influence of these colloidal forces becomes significant. The various forces that enter into the particle-particle interactions and particle-continuous phase interactions are:

- **Electric force** which can be derived from Coulomb's law. It is of the order $\varepsilon\varepsilon_o\psi_S^2$. Where ε is the dielectric constant of the continuous phase and ε_0 is the permittivity of the vacuum. ψ_S gives the surface potential.
- **London-van der Waals force** is produced between macroscopic bodies on the atomic scale and is known as the dispersion force. It is of the order A/a; where A is the Hamaker constant and a gives the characteristic length of the particle.
- **Brownian force** is produced by the thermal energy of the molecules. It is of the order kT/a; where k is Boltzmann's constant and T is the absolute temperature.

- **Viscous force** is increased as the viscosity of the continuous phase increases. The viscous force increases at a rate of μUa; where μ is the continuous phase velocity and U is the particle velocity in the continuous phase.
- **Inertial force** causes by movement of the particles through the continuous phase, of the order $\rho a^2 U^2$; where ρ is the continuous medium density.
- **Surface tension** is produced from particle-continuous phase interaction. This force is of the order γa; where γ is the surface tension of the particle and continuous phase.
- **Gravitational force** shows itself when the density of the particles is higher than the density of the continuous phase. This force acts on the particle of the order $a^3 g\Delta\rho$; where g is the acceleration due to gravity and $\Delta\rho$ is the difference density between solid particle and the continuous phase. When dealing with solid-liquid suspensions this force appears either as a settling velocity or as hindered settling depending on the concentration of the suspension.

a) Settling velocity: When a dense solid particle is placed in a motionless fluid, it will accelerate to a steady-state settling velocity which is called the free settling velocity. It occurs when the drag forces balance the buoyancy and gravitational forces of the fluid on the particle. However, in equilibrium, the sum of these forces is zero.

In Newtonian fluids, for spherical particles the free settling velocity (V_t) is a function of different physical and geometrical parameters (Perry and Green, 1984) and it is defined by:

$$V_t = \left[\frac{4g_c d_P(\rho_s - \rho_l)}{3C_D\rho_l}\right]^{1/2} \qquad [2\text{-}1]$$

where g_c is the gravitational constant, and d_p is the particle diameter, ρ_s and ρ_l are the solid density and suspending fluid density, respectively. In equation [2-1] (C_D) is

the drag coefficient which directly depends on Reynolds number and the particle shape. Reynolds number is the ratio of inertial forces over viscous forces and is defined as:

$$\mathrm{Re}_P = \frac{\rho_l V_t d_P}{\mu} \qquad [2\text{-}2]$$

where μ is the viscosity of the suspending fluid. The expression of drag coefficient for each flow regime is defined in table 2-1

Table 2-1 Hydrodynamic regimes for settling particles (Paul et al., 2004)

Regime	Re_P	C_D
Stokes' law (laminar)	$\mathrm{Re}_P < 0.3$	$C_D = 24/\mathrm{Re}_P$
Intermediate law	$0.3 < \mathrm{Re}_P < 1000$	$C_D = 18.5/\mathrm{Re}_P^{\frac{3}{5}}$
Newton's law (turbulent)	$1000 < \mathrm{Re}_P < 35 \times 10^4$	$C_D = 0.445$

By substituting each definition of drag coefficient in equation 2-1 terminal velocity of droplet V_t for each regime would be obtained:

Stokes' law (laminar regime), $\mathrm{Re}_P < 0.3$:

$$V_t = \frac{g_c d_p^{\,2} (\rho_s - \rho_l)}{18\mu} \qquad [2\text{-}3]$$

Intermediate law (transitional regime) $0.3 < \mathrm{Re}_P < 1000$:

$$V_t = \left[\frac{4g_c}{55.5}\left(\frac{\rho_s - \rho_l}{\rho_l}\right)^{5/7}\right]\left[\frac{\rho_l}{\mu}\right]^{3/7} d_p^{\,8/7} \qquad [2\text{-}4]$$

Newton's law (turbulent regime) $1000 < \mathrm{Re}_P < 35 \times 10^4$:

$$V_t = \left[3d_p g_c\left(\frac{\rho_s - \rho_l}{\rho_l}\right)\right]^{1/2} \qquad [2\text{-}5]$$

b) Hindered settling: In the case of low concentration suspensions, the settling velocity can be evaluated using equations [2-3] to [2-5].However, when the concentration is increased (> 2 %) (Blanc and Guyon, 1991), the particle-particle interactions become significant and other particles decreases the value of V_t. Hindered velocity occurs because of:

(1) Interactions with surrounding particles

(2) Interactions with the upward flow of fluid created by the downward settling of particles

(3) Increases in the apparent suspension viscosity and density.

An empirical correlation for hindered settling velocity is reported by Maude (1958) as:

$$V_{ts} = V_t(1-\phi)^n \qquad [2\text{-}6]$$

where V_{ts} is the hindered velocity, V_t the settling velocity, ϕ the volume fraction of solids in suspension, and n is a function of the particle Reynolds number which is defined as follows:

Table 2-2 Values of the exponent n in Maude (1958) empirical correlation

$Re_p < 0.3$	$n = 4.65$
$0.3 < Re_p < 1000$	$n = 4.375\ Re_p^{-0.0875}$
$Re_p > 1000$	$n = 2.33$

This expression is recommended for preliminary estimates of the effect of solid concentration on settling velocity.

2.1.3 Rheological properties of suspension

Rheology is the science of flow and deformation of materials. The rheology of suspensions is an important subject in the field of rheology since it shows various types of exceptional rheological characteristics such as thixotropy, shear thinning, shear thickening, etc. We need to develop our knowledge about suspension rheology for a wide range of industrial applications such as paint, ink, cement, cosmetics, food, and agricultural products in order to select the best production condition for the specific application.

Jinescu (1974) classifies suspensions depending on the rheological behavior of the continuous phase. These classifications are given below.

2.1.3.1 Suspensions in a continuous Newtonian phase

For suspensions in which the continuous phase is Newtonian, Newtonian behavior can be seen for small concentrations of solid particles. Generally, a Newtonian suspension is not applicable when the concentration of solid particles exceeds 37%. It has been found that the variation of viscosity with solid particle concentration is determined from a value defined as the critical concentration. For values higher than the critical concentration, the viscosity of the suspension increases with concentration, due to

particle-particle interactions. The critical concentration for each suspension depends on the nature, shape and dimensions of the solid particles. For example, for glass rods the critical concentration is 15% by volume and for spherical polymethyl methacrylate this value is 40% by volume.

2.1.3.2 Suspensions in a continuous non-Newtonian phase

This type of suspension shows non-Newtonian behavior even with small concentrations of solid particles. In small solid particle concentrations, the non-Newtonian behavior is caused by the continuous phase. However, with high concentrations of solid particles, particle-particle interactions accentuate the non-Newtonian behavior of the suspensions. In these types of suspensions, the rheological behavior depends on the nature, shape, dimensions, and concentration of the solid phase, the rheological nature of the liquid phase and possibly on time.

2.1.3.3 Relative viscosity of suspensions

Much experimental and theoretical work has been carried out to predict the rheological behavior of suspensions,. The theoretical correlation proposed by Einstein (1906-1911) is known as the first on this subject. Einstein derived this correlation to predict the viscosity of dilute suspensions. The Einstein equation is

$$\mu_r = \frac{\mu_{eff}}{\mu_0} = \left(1 + \frac{5}{2}\varphi\right) \qquad [2\text{-}7]$$

where μ_r is relative viscosity, ϕ is the volume fraction of the spheres, μ_{eff} is effective viscosity and μ_o is the viscosity of the continuous phase. The equation indicates that the relative viscosity is independent of particle size. Einstein considered a suspension of

rigid spheres, so dilute that the movement of one sphere doesn't influence the fluid flow in the neighborhood of any other spheres.

As the particle concentration increases and particle-particle interaction becomes non - negligible, the relation between the relative viscosity and volume fraction starts to deviate from linearity. Guth and Gold (1977) added a quadratic term to the Einstein equation for slightly higher particle concentrations

$$\mu_r = \left(1 + 2.5\phi + 14.1\phi^2\right) \qquad [2\text{-}8]$$

These two models are derived under the assumption of spherical, rigid and monodisperse particles.

As the particle concentration increases ($\varphi > 10\%$) and particle-particle interactions in the suspension are no longer negligible, the rheological properties of the suspension become more complex. A number of equations have been developed to interpret the concentration dependence of concentrated suspensions theoretically and experimentally. Eiler (1941), developed an equation for concentrated suspensions as follows:

$$\mu_r = \left(1 - \frac{2.5\phi}{2(1 - b\phi)}\right)^2 \qquad [2\text{-}9]$$

Where $b = 1/\phi_m$ and ϕ_m is the apparent maximum packing volume fraction which reflects the state of aggregation. Another semi empirical equation has been developed by Mooney (1951). The Mooney equation is

$$\mu_r = \exp\left(\frac{\frac{5}{2}\phi}{1 - \left(\phi/\phi_0\right)}\right) \qquad [2\text{-}10]$$

In this equation ϕ_o is an empirical constant between about 0.74 and 0.52, with these values corresponding to the values of ϕ for closest packing and cubic packing, respectively.

The phenomenological model of Krieger-Dougherty (1959) is frequently used in concentrated suspensions of nonspherical particles

$$\mu_r = \left(1 - \phi/\phi_m\right)^{-A\phi_m} \qquad [2\text{-}11]$$

Where (ϕ_m) is the maximum volume fraction of particles that the suspension can contain. This parameter is a function of the particle's shape and its granulometry (polydispersity). The parameters A and ϕ_m are tabulated in table 2-3 for suspension of several materials.

Table 2-3 Dimensionless constant used in Krieger-Dougherty equation for different systems (Bird et al., 1960)

System	A	ϕ_{max}
Spheres(submicron)	2.7	0.71
Spheres (40 μm)	3.28	0.61
Ground gypsum	3.25	0.69
Glass rods (30×70 μm)	9.25	0.268
Glass plates(30×70 μm)	9.87	0.382
Glass fibres (axial ratio 7)	3.8	0.374
Glass fibres (axial ratio 14)	5.03	0.26
Glass fibres (axial ratio 21)	6.0	0.233

Maron and Pierce (1956) derived another equation which is very similar to the Krieger-Dougherty equation

$$\mu_r = (1 - \phi/A)^{-2} \qquad [2\text{-}12]$$

where A is a constant relating to the packing geometry of the particles.

Quemada's phenomenological approach (1986) is interesting due to the fact that it is based on the optimization of viscous energy dissipation

$$\mu_r = \left(1 - \frac{1}{2} k\phi\right)^{-2} \qquad [2\text{-}13]$$

where k is a structural parameter, closely associated with packing concentration φ_M in Newtonian regimes, where

$$k = 2/\varphi_M \qquad [2\text{-}14]$$

The recent study by Gillies et al. (1999) shows that the viscosity of a suspension which contains a volume concentration of spherical solid particles up to 50% is in good agreement with the experimental results from the correlation proposed by Thomas (1965)

$$\mu_r = 1 + 2.5\varphi + 10.06\varphi^2 + 0.00273\exp(16.6\varphi) \qquad [2\text{-}15]$$

where the terms of order two and higher are a result of particle-particle interactions in highly concentrated suspensions.

All the models mentioned above are proposed models for predicting the relative viscosity of a Newtonian suspension. The particle was rigid and no effect of shear rate on the viscosity of suspension has been revealed.

In colloidal suspensions where the colloidal interactions become significant, the rheology of suspensions is complex. In these types of suspensions, aggregation, orientation, the deformation of particles, the effect of shear rate and possibly shearing time are no longer negligible.

Figure 2-1 presents the typical viscosity behavior of colloidal suspensions as a function of shear rate and volume fraction of particles in steady-state regime (Shamlou, 1993).

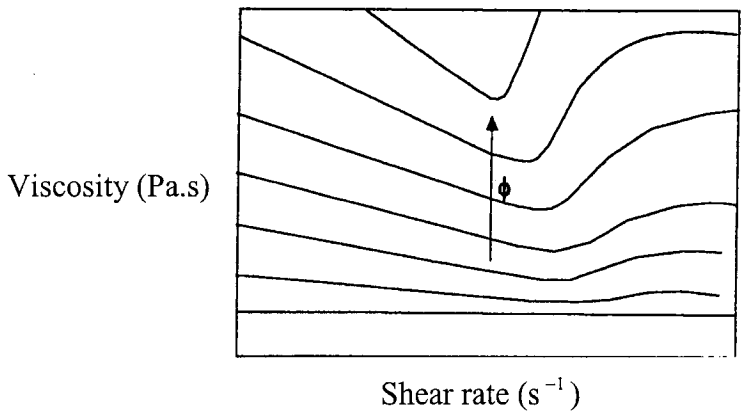

Figure 2-1 Typical behavior of viscosity of suspensions

In low shear rate, the effect of shear thinning would be observed, meaning that the viscosity decreases with increasing shear. Shear thinning is most frequently encountered with concentrated suspensions. Drawing on the unit structural concept (the aggregates), Quemada believes that the viscosity reduction is due to desegregation of flakes when the shear rate increases. At high shear rates, the effect of shear thickening appears. Figure 2-1 shows that at very high suspension concentrations, only a small increase in shear rate is required to change a nondilatant behavior into a strongly dilatant (shear thickening) one.

The shear thinning viscosity part of the curve may be represented by means of many available models in literature; Carreau model, Cross or Ostwald-De-Waele (power law) (Shamlou, 1993). In order to explain this rheological behavior of concentrated suspensions, Quemada (1978) developed a semi-empirical model with 4 parameters which is derived from Newtonian equation:

$$\eta = \eta_f \left[1 - \frac{\phi}{2} \left(k_\infty + \frac{1}{1 + \left(\frac{\dot{\gamma}}{\dot{\gamma}_c} \right)^p} (k_0 - k_\infty) \right) \right]^{-2} \qquad [2\text{-}16]$$

where η_f is the viscosity of the suspending fluid, k is the intrinsic generalized Quemada's viscosity with the limiting values of k_0 and k_∞ for a low shear rate and high shear rate and p represents the structural parameter.

Finally, many authors have produced works concerning the rheological behavior of concentrated colloidal suspensions. Alessandrini et al. (1982), mentioned that kaolin suspensions in aqueous mediums have shear thinning effects. These suspensions have delicate structures which are affected by the shear rate. This structural modification takes place gradually with time. Also, these authors demonstrate that these suspensions have a force threshold below which they do not flow at all and behave as solids.

2.2 Solid-liquid suspension in mechanically agitated vessels

2.2.1 Hydrodynamic regimes

In order to disperse and distribute solid particles throughout a vessel, they should first be lifted up from the vessel bottom, requiring suitable velocities and turbulence levels in that region. Nienow (1985) discussed in some detail the hydrodynamic interactions between solid particles and fluids in mechanically agitated tanks. First, there is a drag force on particles arising from boundary layer flow across the bottom of the tank. The velocity of the boundary layer flow should be ten times greater than the particle settling velocity in a motionless fluid to suspend the particle. Second, turbulence breaks the boundary layer and if the frequency and energy levels are high enough, a suspension will be started.

Among the various models for particle suspension, the most successful was proposed by Baldi et al. (1978). According to this model the suspension of the particles at rest in certain zones near the tank bottom is mainly due to turbulent eddies of approximately the same scale as the particle size.

2.2.2 N_{js} just suspension speed in stirred tanks

It has long been recognized that the impeller speed at which particulate solids just begin to become fully suspended is the most important speed. At this speed the maximum surface area of the particles is exposed to the fluid for chemical reaction or mass or heat transfer. Hence this is an important characteristic to understand in order to make sure that our mixing process is working in rotational speed below or equal or above the threshold suspension speed.

2.2.2.1 N_{js} correlations

There have been lots of experimental and theoretical studies to quantify the value of N_{js}. Zwietering (1958) derived the following correlation from dimensional analysis. He estimated the exponents by fitting the data to the just-suspended impeller speed:

$$N_{js} = S\upsilon^{0.1}\left[\frac{g_c(\rho_s - \rho_l)}{\rho_l}\right]X^{0.13}d_p{}^{0.2}D^{-0.85} \qquad [2\text{-}17]$$

where:

$$S = \mathrm{Re}_{imp}{}^{0.1}\,Fr^{0.45}\left(\frac{D}{d_p}\right)^{0.2}X^{0.13} \qquad [2\text{-}18]$$

where:

$$\mathrm{Re}_{imp} = \frac{N_{js}D^2}{\upsilon} \qquad [2\text{-}19]$$

is the impeller Reynolds number

$$Fr = \frac{\rho_l N_{js}{}^2 D}{(\rho_s - \rho_l)g_c} \qquad [2\text{-}20]$$

is the Froude number

- D : impeller diameter
- d_p : mass-mean particle diameter
- X : mass ratio of suspended solids to liquid
- N_{js} : impeller speed for just suspended
- υ : kinematic viscosity of the liquid
- g_c : gravitational acceleration
- ρ_s and ρ_l : density of the particles and density of the liquid

The approach by Zwietering does not, however, provide an understanding of the phenomenon of particle suspension. For this purpose different models have been proposed.

Narayanan et al. proposed a theoretical expression for N_{js}, derived balancing the vertical forces acting on the particle: the downward gravity force and the upward drag force due to the vertical component of the fluid velocity.

Kolar assumed that the mixing energy necessary to suspend a particle equals the energy dissipated by the particle moving at its terminal velocity in a motionless fluid.

Although much of the work in solid – liquid suspension is related to minimum impeller speed, in this state, the distribution of solids over the vessel may be extremely non-uniform. The distribution of solids must be treated differently from the suspension.

2.3 Solid-liquid dispersion in high viscous continuous phase

In the previous section the continuous phase viscosity was considered to be low enough to reach a turbulent regime. In the aforementioned systems, obtaining a uniform suspension is a difficult task due to the high settling velocity of the particles and the need for turbulent eddies. However, in many industrial processes like plastics, food, rubber and pastes, the continuous phase viscosity is extremely high. In cases such as

these, the viscosity of the system is too high to reach turbulent regime and agitation of such systems leads to a laminar regime. Processing of these high viscosity materials may require the incorporation of fine solids. To achieve a solid dispersion into a viscous continuous phase, the objective is to produce a uniform material with an acceptably low level of agglomerates of the basic individual particles.

In high viscosity continuous phases, in the absence of turbulent eddies, the stresses which are produced within the liquid during laminar flow are responsible for breaking and rupturing agglomerates of particles and dispersing them uniformly as individual particles throughout the vessel. In the absence of molecular diffusion, this mechanism tends to reduce the size and scale of the unmixed clumps. High shear stresses for such a task can be achieved in mixers which provide high shear and the components should pass through these zones as often as possible. In mixers handling high viscosity fluids (such as Kneaders, internal mixers, planetary mixers, and helical ribbons) the flow patterns are very complex. All of these mixers incorporate high shear zones and regions where fluids are redistributed. However, the shear produced in the high shear zones of these mixers may not be enough to reduce the size of the agglomerates and break the lumps as required. In this case, incorporation of a high shear mixer and a distributive mixer for high viscosity continuous phases would improve the mixture quality.

2.3.1 Disperser turbine for concentrated solid-liquid dispersion

In the previous chapter, the most common high speed dispersers (Cowles or sawtooth disperser) which produce high shear were presented. It was also mentioned that the role of these types of impellers is to break up the agglomerates and reduce the particle size within the dispersion. Although these types of dispersers are known to provide sufficient dispersing capabilities, they must be operated at very high rotational speeds and exhibit high power consumption. In order to reduce the power consumption of this type of disperser, Furling et al., (2001) develop a new impeller technology. They characterized

the performance of the new impellers, called the Deflo and sawtooth impellers in terms of the power consumption and mixing quality in a high pigment slurry concentration (70 wt %). The Deflo turbine is a modified sawtooth impeller with a reduced number of teeth and with tooth-orientation permitting better pumping capacity.

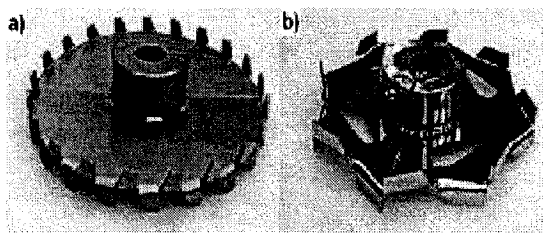

Figure 2-2 Dispersion impellers: (a) Cowles impeller, (b) Deflo impeller

The results of their experiments revealed that the Cowles impeller is an adequate tool for high solid concentration pigmented slurries. However, the power consumption is significantly high. In contrast, the Deflo impeller requires less power consumption while the shear level and the pumping capacity is high enough to incorporate the pigments throughout the vessel and break the agglomerates.

2.3.2 Atypical helical ribbon impeller (Paravisc)

High viscosity mixing is commonly encountered in most chemical and food industries. The mixing systems which are used for mixing high viscosity fluids should have the capability of circulating the entire vessel contents and avoid cavern effects. Close-clearance impellers such as anchor and helical ribbon impellers, are examples of such mixers. Delaplace et al., (2000) have studied the power consumption and homogenization performance of atypical helical ribbon impellers (the Paravisc system from Ekato). This new impeller has two advantages compared to typical double helical ribbon impeller: first, the bottom of this impeller is equipped with an anchor, preventing formation of stagnant zones; second, the size of pitch ratio of the Paravisc is higher than typical double helical ribbon impellers, providing a higher shear rate. The experimental

studies on the performance of the Paravisc and double helical ribbon impellers show interesting results. Evaluations of the circulation time for both impellers reveals that the pumping capacity of the Paravisc has not been improved by using a higher pitch ratio. Furthermore, the power consumption with the Paravisc is higher compared to double helical ribbon impellers due to the additional anchor at the bottom. However, this anchor-equipped bottom of the Paravisc impeller is well adapted to mixing high viscosity solid-liquid dispersions since the design avoids the formation of dead zones resulting from sedimentation effects.

2.3.3 Power consumption

2.3.3.1 Power consumption in Newtonian fluids

An agitator's power consumption is a decisive factor in its design. In mixing studies, the variables are often manipulated to create dimensionless numbers. These dimensionless numbers take into account the geometry of the mixing system, the rheology of the fluid and the flow dynamics (Holland and Chapman, 1996). Two dimensionless numbers which are used are the Power number (N_P) and Reynolds number (Re):

$$N_p = \frac{P}{\rho N^3 D^5} \qquad [2\text{-}21]$$

where P represents the power consumption by the impeller, ρ is the density of the fluid, N is the impeller's rotational speed and D is the impeller's diameter.

For constant geometrical relationships and negligible gravitational influence, the power number depends only on the impeller Reynolds number:

$$\mathrm{Re} = \frac{\rho N D^2}{\mu} \qquad [2\text{-}22]$$

where μ is a Newtonian viscosity. In a laminar regime the power number is inversely proportional to Reynolds number,

$$N_P = \frac{K_P}{\mathrm{Re}} \qquad [2\text{-}23]$$

where K_P is a constant which depends on the geometry of the mixing system. In a transitional regime there is no simple expression for N_p vs. Re. Generally, the anchor agitator operates in laminar regime for Reynolds numbers lower than 100 and for larger values the flow becomes transitional. For dispersion impellers when Reynolds is lower than 10 the agitator operates in laminar regime and becomes turbulent for Reynolds greater than 4500 (Foucault et al., 2004).

2.3.3.2 Power consumption in non-Newtonian fluids

As mentioned previously, predicting the power consumption for Newtonian fluids is relatively simple. For non-Newtonian fluids where the apparent viscosity of the fluid changes as the shear rate changes, determining the power consumption is complicated. In fact, in non-Newtonian fluids the viscosity is no longer constant. The viscosity varies with the applied shear rate on the fluid. A means of dealing with this difficulty was first proposed by Metzner and Otto (1957) for non-Newtonian fluid in laminar regime based on calculations of apparent viscosity for mixers. The basic assumption of this method is that there is an effective shear rate for a mixer which can describe the power consumption and this shear rate is proportional to impeller speed:

$$\dot{\gamma}_e = K_s N \qquad [2\text{-}24]$$

where K_s is a shear rate constant which depends on the geometry of the impeller and $\dot{\gamma}_e$ is an effective shear rate which defines an apparent viscosity for predicting power

consumption in non-Newtonian fluids. In order to determine the value of K_s, the following steps are proposed:

- For a specific rotational speed (N), the power consumption can be determined experimentally, and the power number for non-Newtonian fluids can be calculated from equation [2-21].
- From the Newtonian power curve, find the Reynolds number corresponding to the non-Newtonian power number. This Reynolds number is known as the generalized Reynolds number (Re_g). The apparent viscosity is calculated from the following equation:

$$\mathrm{Re}_g = \frac{\rho N D^2}{\eta_a} \qquad [2\text{-}25]$$

- From the curve of viscosity vs. shear rate which can be obtained experimentally, the shear rate can be found according to the apparent viscosity.
- Finally, the slope of effective shear rate vs. rotational speed gives the value of K_s.

The value of K_s, can also be determined by mathematical manipulation. By substituting Newtonian viscosity (μ) by the apparent viscosity of the non-Newtonian fluid (η_a) in the expression for K_p (due to the fact that our non-Newtonian fluids obey the power law $\eta = m|\dot{\gamma}|^{n-1}$) we obtain

$$N_p = \frac{K_p}{\mathrm{Re}} = \frac{K_p m (K_s N)^{n-1}}{\rho N D^2} = \frac{K_p K_s{}^{n-1}}{\mathrm{Re}_{pl}} \qquad [2\text{-}26]$$

Using the fact that $K_p(n) = N_p.\mathrm{Re}_{pl}$

$$K_s = \left(\frac{K_p(n)}{K_p} \right)^{\frac{1}{n-1}} \qquad [2\text{-}27]$$

This method can also be generalized to Bingham fluids and Hershel-Bulkley fluids. From these correlations, two power measurements, one for Newtonian fluids and one for non-Newtonian fluids of known viscosities, are enough to obtain K_s.

When designing a process system, the selection of the most appropriate mixing system according to the process specifications is a significant task. The selection criterion is often based on mixture quality (homogenization) and power consumption (Holland, Chapman, 1966).. In order to predict the performance of a mixing system many studies characterize the power consumption and mixing time of that system.

Pahl et al., (1996) have characterized the power consumption of a triple shaft mixer. Figure 2-3 shows the triple shaft mixer apparatus used in this study.

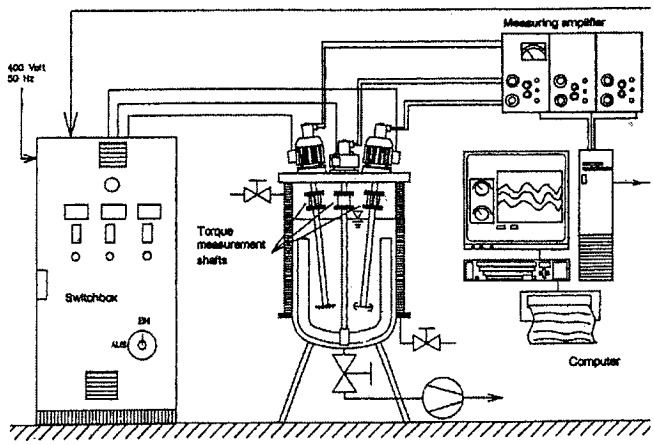

Figure 2-3 Schema of the triple shaft mixer (Pahl et al., 1996)

The mixer is equipped with an anchor impeller, a toothed disc and a propeller. Each agitator is supplied by their own drive unit in order to study the power consumption of each agitator and the interaction between the impellers. The experimental results show that the power consumption of the anchor drops sharply as the Reynolds number of the

toothed disc and the propeller is increased. However, the influence of the toothed disc on the power consumption of the anchor impeller is more noticeable compared to propeller. This observation can be explained by the fact that both the toothed disc and propeller support the anchor in churning the entire vessel contents. Moreover, as the main direction of action of the propeller is axial and the toothed disc's is tangential, the anchor's power consumption is more affected by the toothed disc. In another part of the work by Pahl et al. (1996), the power consumption of the toothed disc and propeller was studied individually and in the triple shaft system. Although the power consumption of each impeller is smaller in the triple-shaft operation compare to single-shaft operation, the total power consumption of the triple-shaft mixer is higher. In order to clarify the experimental results for the power consumption of each impeller in the triple-shaft mixer, Pahl et al. (1996) have proposed a model. As previously noted, in laminar regime in the single-shaft mixer, the power number can be determined from equation [2-21]. In the case of the multi-shaft mixer in laminar regime, the influence of additional impellers can be superimposed and expressed using the following equation:

$$N_P = \frac{A - \sum \varphi_i^{a_i}}{\mathrm{Re}} \qquad [2\text{-}28]$$

where

$$\phi_i = \frac{n_i}{n} \qquad [2\text{-}29]$$

where N is the rotational speed of the impellers.

In single-shaft system in turbulent regime, Nagata (1975) have shown that:

$$N_P = B\left(\frac{10^3 + f\,\mathrm{Re}^{\alpha}}{10^3 + h\,\mathrm{Re}^{\alpha}}\right)^{\beta} \qquad [2\text{-}30]$$

They proposed that, as in the turbulent regime, the interaction between the stirrers is negligible and the theorem of Nagata is still valid. Thus a generalized description for the power number in the multi-shaft agitator can be taken as:

$$N_P = \frac{A - \sum \varphi_i^{a_i}}{\mathrm{Re}} + B\left(\frac{10^3 + f\,\mathrm{Re}^{\alpha}}{10^3 + h\,\mathrm{Re}^{\alpha}}\right)^{\beta} \qquad [2\text{-}31]$$

In this work each coefficient of the generalized description has been obtained using experimental data. The correlations obtained by the authors for triple-shaft mixers are:
For the anchor :

$$N_P = \frac{103.5 - \left(\frac{n_P}{n_A}\right)^{0.69} - \left(\frac{n_Z}{n_A}\right)^{0.84}}{\mathrm{Re}_A} + 4.9\left(\frac{10^3 + 43.3\mathrm{Re}_A^{\,0.33}}{10^3 + 259.8\mathrm{Re}_A^{\,0.33}}\right)^{2.09} \qquad [2\text{-}32]$$

For the propeller:

$$N_P = \frac{26.8 - \left(\frac{n_A}{n_P}\right)^{0.75} - \left(\frac{n_Z}{n_P}\right)^{0.49}}{\mathrm{Re}_P} + 0.53\left(\frac{10^3 + 3.0\mathrm{Re}_P^{\,0.72}}{10^3 + 4.0\mathrm{Re}_P^{\,0.72}}\right)^{1.72} \qquad [2\text{-}33]$$

For the toothed disc:

$$N_P = \frac{41.5 - \left(\frac{n_A}{n_Z}\right)^{0.28} - \left(\frac{n_P}{n_Z}\right)^{0.30}}{\mathrm{Re}_Z} + 32.8\left(\frac{10^3 + 371.7\mathrm{Re}_Z^{\,0.37}}{10^3 + 1585.5\mathrm{Re}^{0.37}}\right)^{2.89} \qquad [2\text{-}34]$$

As mentioned in the first chapter, one of the most common mixers used in the process industry is the double planetary mixer. This type of mixer was originally used for propellant mixing and subsequently found other applications in the adhesive, food and cosmetic industries with the extremely high viscosity mediums. In order to investigate the hydrodynamic performance of the double planetary mixer, Tanguy et al., (1999) evaluated the dispersive and distributive mechanisms generated by rotating arms both numerically and experimentally. Figure 2-4 provides a picture of the double planetary mixer. This mixer consists of two scrapping arms (anchor impeller) mounted on a rotating carousel in an off-centered position.

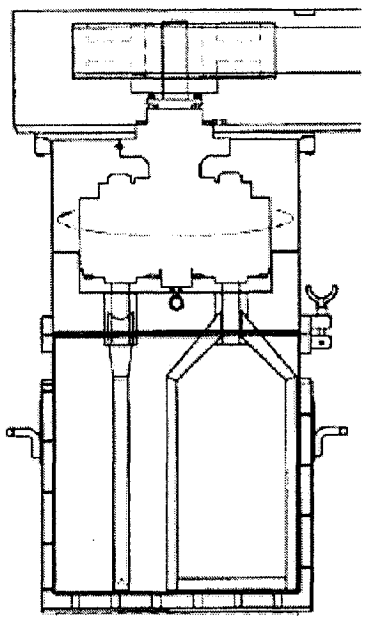

Figure 2-4 Schema of a double planetary mixer

At a constant rotational speed of the carousel (10 rpm) it has been shown numerically and experimentally that the mixer provides good radial dispersion. However, in terms of axial (top-to-bottom) pumping, it was shown that a significant time is needed for particles to cross the upper half of the vessel when the particles are injected at the surface. Nevertheless, due to the action of the anchor impellers horizontal arms, good axial dispersion at the bottom of the vessel is achieved. In this study, at conversion

levels up to 70%, very good agreement between the numerical prediction and experimental results was observed. At 80% conversion the model is not accurate enough to predict the power consumption, due to the fact that the free surface of the fluid is no longer flat and that the shear thinning character of the fluid has not been considered in the computations,.

Thibault and Tanguy (2002) studied the power consumption of a new coaxial mixer composed of a wall-scraping arm with a series of rods and a pitched blade turbine mounted on a same axis of revolution which operated in a counter-rotating mode.

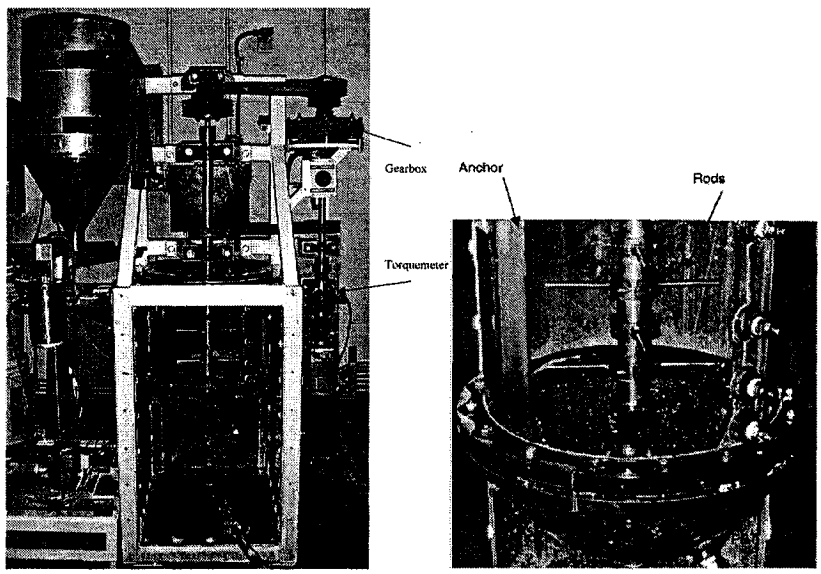

Figure 2-5 Experimental coaxial mixer setup (Thibault et Tanguy, 2002)

They found that the power was a function of the speed ratio of the fast agitator to the slow agitator in both laminar and turbulent regime. In laminar regime in Newtonian mediums they determined the correlations which predict the power constant $K_{Panchor}$ and $K_{rods+PBT}$. These correlations are functions of the speed ratio $(R_N = N_t / N_a)$ between the two agitators.

$$K_{Panchor}(R_N) = 26.09R_N^{\,2} + 88.66R_N + 256 \qquad 0 \le R_N \le 24 \qquad [2\text{-}35]$$

$$K_{Prods+PBT}(R_N) = 829.04/R_N^{\,2} + 330.56/R_N + 99 \qquad 4 \le R_N \le \infty \qquad [2\text{-}36]$$

From these two correlations it is possible to determine the total power consumption of the coaxial mixer. According to the selected K_P (anchor or rods+PBT), the power consumption can be determined using equation [2-39].

In the case of Non-Newtonian fluids (power law type), they showed that the values of $K_{Panchor}$ and $K_{rods+PBT}$ could be expressed as functions of the speed ratio and fluid flow index (n).

$$K_{Panchor}(R_N, n) = \frac{P_{tot}}{kN_a^{\,n+1}D_a^{\,3}} = 256e^{-3.12(1-n)} + 88.66e^{-2.97(1-n)}R_N + 26.09e^{-6.61(1-n)}R_N^{\,2} \qquad [2\text{-}37]$$

$$0 \le R_N \le 24$$

$$K_{Ptiges+PBT}(R_N, n) = \frac{P_{tot}}{kN_t^{\,n+1}D_t^{\,3}} = 99e^{-2.18(1-n)} + \frac{330.56e^{-2.25(1-n)}}{R_N} + \frac{829.04e^{-3.72(1-n)}}{R_N^{\,2}} \qquad [2\text{-}38]$$

$$4 \le R_N \le \infty$$

For the same coaxial system they showed that the total power curves in turbulent regime vary with the speed ratio. These power correlations, similar to the laminar regime case, are developed for both agitators.

$$N_{Panchor}(R_N) = 0.1936R_N^{\,2.7838} \qquad 4 \le R_N \le 24 \qquad [2\text{-}39]$$

$$N_{Prods+PBT}(R_N) = -4.4238/R_N^{\,2} + 3.3176/R_N + 0.74 \qquad 4 \le R_N \le \infty \qquad [2\text{-}40]$$

These two equations can be used to estimate the total power consumption of the system from equation [2-37].

Another interesting power consumption characterization study was carried out by Foucault et al. (2004). They used a coaxial mixer with two independent torque meters in order to characterize the power consumption of each agitator. This coaxial mixer consisted of an anchor and different dispersion turbines mounted on the same shaft. To determine the best agitation mode for the agitators both the co-rotating and counter-rotating modes have been studied.

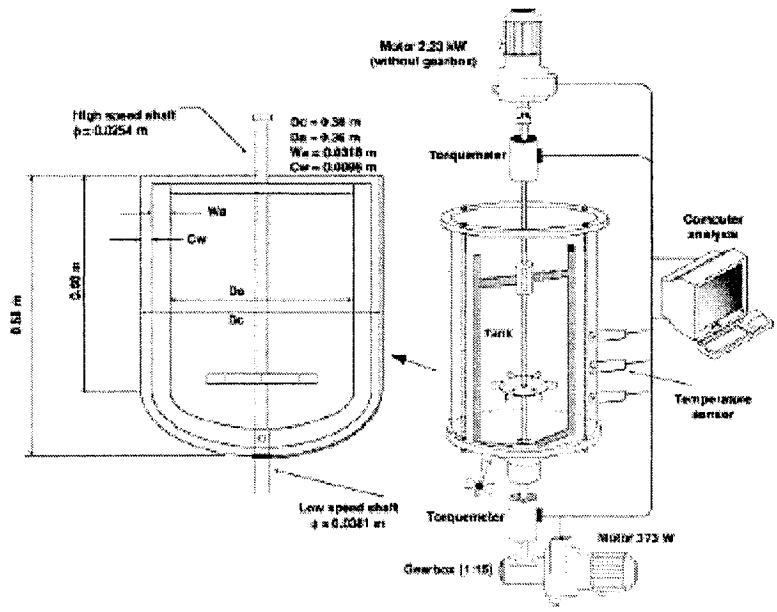

Figure 2-6 Experimental coaxial mixer setup (Foucault et al., 2004)

They found that the anchor power draw increases with the dispersing turbine in contra-rotating mode and decreases in co-rotating mode. However, contrary to the anchor power consumption, the disperser power draw is not affected by the anchor speed.

They have determined in laminar and turbulent regime that the variation of the total power constant ($K_{Panchor}$) and ($N_{Panchor}$) exhibits a polynomial dependence on the speed ratio.

$$K_{Panchor}(R_N) = 13.16R_N^{\,2} + 9.74R_N + 230 \qquad 0 \le R_N \le 30 \qquad [2\text{-}41]$$

$$N_{Panchor}(R_N) = 0.62R_N^{\,2.27} \qquad 0 \le R_N \le 30 \qquad [2\text{-}42]$$

These two equations allow the estimation of the coaxial mixer (Rushton turbine – anchor) power draw for Newtonian fluids as a function of the speed ratio in contra-rotating mode. The study takes an interesting approach in modifying the definition of Reynolds number and the power number for this coaxial mixer. Considering the independence of the central agitator's power draw from the speed ratio, the coaxial mixer's power draw can be correlated with the characteristic impeller diameter. The Reynolds number can then be modified according to the rotational mode. The following equations express the Reynolds number used to determine the coaxial mixer curve in Newtonian and Non-Newtonian fluids.

$$\mathrm{Re}_{(conta-rotation)} = \frac{\rho \times (N_t + N_a) \times D_t^2}{\mu} \quad [2\text{-}43]$$

$$\mathrm{Re}_{(co-rotation)} = \frac{\rho \times (N_t - N_a) \times D_t^2}{\mu} \quad [2\text{-}44]$$

$$\mathrm{Re}_{(contra-rotation)} = \frac{\rho \times (N_t + N_a)^{(2-n)} \times D_t^2}{k} \quad [2\text{-}45]$$

$$\mathrm{Re}_{(co-rotation)} = \frac{\rho \times (N_t - N_a)^{(2-n)} \times D_t^2}{k} \quad [2\text{-}46]$$

where N_t is the turbine speed, N_a is the anchor speed and D_t is the characteristic diameter.

The same reasoning can be used to calculate the total power number of the system in counter-rotating and co-rotating modes.

$$N_{P(contra-rotating)} = \frac{P_{tot}}{\rho \times (N_t + N_a)^3 \times D_t^5} \quad [2\text{-}47]$$

$$N_{p(co-rotating)} = \frac{P_{tot}}{\rho \times (N_t - N_a)^3 \times D_t^5} \quad [2\text{-}48]$$

It must be mentioned that the new correlations are only valid for speed ratios higher than 10.

2.3.3.3 Power consumption in suspension

Few investigations have dealt with the characterization of N_p and Re for suspensions. Pasquali et al (1983) was the first to estimate the power curve for suspensions of rigid, spherical particles of uniform size with maximum 30 % volume of solid concentration in Newtonian fluids. Afterwards, for solid – liquid suspensions, they introduced the modified power number and modified Reynolds number as following:

$$N_P{}^* = \frac{P}{\rho^* N^3 D^5} \qquad [2\text{-}49]$$

$$\mathrm{Re}^* = \frac{\rho^* N D^2}{\mu^*} \qquad [2\text{-}50]$$

where ρ^* is density and μ^* is the viscosity of the suspension. These two parameters are defined as follows:

$$\rho^* = \phi_v \rho_s + (1-\phi_v)\rho_l \qquad [2\text{-}51]$$

$$\mu^* = \mu_l\left(1 + 2.5\phi_v + 10.05\phi_v{}^2 + 0.00273\exp(16.6\phi_v)\right) \qquad [2\text{-}52]$$

where ϕ_v is the solid volume concentration, ρ_s is the density of the solid particles, ρ_l and μ_l are the density and viscosity of the continuous phase, respectively.

In this manner, they observed that the modified power curve ($N_P{}^*$ vs Re^*) superimposes the single phase power curve (N_P vs Re). Consequently the power consumption of solid – liquid mixing can be estimated if the single phase power curve is known, as well as the density of the suspension (defined as the total mass in the vessel divided by the total volume) and the volume fraction of particles.

2.3.4 Solid distribution

The first requirement for solid-liquid mixing is complete off-bottom suspension. The second requirement is an even distribution of solids within the tank. In this section, the techniques which give either accurate quantitative data on local concentration of solids, or general observations and semi-quantitative information on the distribution of solids are described.

Visual observation is a useful means of roughly estimating the degree of homogeneity in a mixing tank. Observation of multiphase flow is necessary in order to choose the best position for locating the instruments in the tank. It also helps us to identify problems such as stagnant areas where solids may collect. Despite the advantages of visual observation, this technique won't help in high solid concentration systems, where solids screen most of the tank from view. Visual investigation of mixing mechanisms may be possible at lower solid concentration, but flow pattern observations should be carried out at high concentrations due to the fact that flow patterns change considerably with solid concentration.

The use of a conductivity probe is useful for obtaining precise and accurate information about local solid concentration. This method can be used where the suspending fluid is conductive and the suspended solids are nonconductive. Because the conductive probe must be placed within the tank, it has the disadvantage of being intrusive as well as altering the flows and possibly the solid concentration at the measuring point. As the solids concentration of the probe volume changes, the electrical conductivity of the probe volume changes too. The measured conductivity of the probe volume and the volume fraction of solids have the following relation:

$$\frac{\kappa}{\kappa_O} = 1 - A\varepsilon_S \qquad [2\text{-}53]$$

where κ is the measured conductivity, κ_O is the conductivity in the absence of solids, ε_S is the volume fraction of solids, and A is a calibration factor.

The measured conductivity not only changes as a function of solid concentration, but also due to changes in the fluid temperature and dissolved impurities. During use the temperature should be measured accurately, and any changes should be corrected by the following expression:

$$\kappa_C = \kappa_M \frac{\kappa_{OR}}{\kappa_{OM}} \qquad [2\text{-}54]$$

where κ_C is the conductivity corrected to the reference temperature, κ_M the measured conductivity, κ_{OR} the fluid conductivity at the reference temperature, and κ_{OM} the fluid conductivity at the measured temperature. The conductivity probe is a useful method at the laboratory scale, however, with special precautions it can be used in industrial plants as well.

Optical probes are another instrument for measuring solids concentration. Generally there are two types: light absorption and light scattering. In both types the amount of light absorbed or scattered is related to the solid concentration. Using Beer's law we have:

$$\log \frac{I_0}{I} = E \varepsilon_S \ell \qquad [2\text{-}55]$$

Where I_0 is the intensity of the incident light, I is the light intensity after absorption, E is the extinction coefficient for the system, ε_S is the volume fraction of solids and ℓ is the optical path length. The extinction coefficient is a function of particle size and wavelength, which themselves affect the relative amounts of light absorbed and scattered.

Temperature variations and impurities do not affect the absorbed or scattered light. However, as the probe response is a function of both particle size and solid concentration, distinction between the two effects is impossible. Because the particle size distribution varies with position in the tank, the probe response would be a function of position in the tank. The optical probe is less interfering than the conductivity probes. Accurate and precise measurements would be obtained if calibration is carried

out. Generally, they are used in laboratory conditions, but in some cases they may be used in industrial process plants at low concentrations of solid particles, as the measurements are extremely difficult at solids concentrations of more than 2 to 3 vol %.
Direct sampling is a very useful method for cases where information about particle size distribution or solid concentration is needed. The particle size distribution can be determined by means of master sizer and the local concentration can also be obtained by measuring the amount of solids that the sample contains.
Two methods exist for removing a sample from the tank: pump the sample out through a pipe or take a grab sample. Removal of samples through a pipe should be performed isokinetically, meaning that the velocity of the sample which enters the pipe must be the same as the local fluid velocity, and the pipe must be aligned in the local direction of the flow.
Grab sampling is performed by means of immersing a container fitted with a lid into the tank. The lid is opened slightly in order to fill the container, then the lid is closed and the container is removed to withdraw the sample. This technique can be applied in many situations, as it can be done even at high solid concentrations. The major disadvantage of this technique is that the equipment is not commercially available. Thus, the required equipment has to be designed and built for each job.
Electrical tomography is a nonintrusive method which measures the local velocity, density and concentration in three dimensions. This method is the most widely used for stirred vessels.

2.3.5 Mixing time

Mixing time is defined as the time necessary to reach a certain degree of local homogeneity. Qualitative mixing time measurement which gives us a qualitative understanding of mixing behavior could be obtained by the decolorization technique. In this technique the entire contents of the tank are colored using one chemical, and then a

second is added to remove the color. pH changes using an appropriate indicator and an iodine-iodide change in the presence of starch are the two most common reactions. Bromophenol blue (blue to yellow) or phenolphthalein (pink to colorless) are two common indicators which can be added to the tank. Small amount of acid can be used in order to color the entire tank and then strip out the color. Another decolorization reaction is between sodium thiosulfate and iodine in the presence of starch. The color change is from deep blue to clear. In this method the mixing time is defined from the time that the impeller starts to rotate until the color of the tracer in the entire tank strips out and the fluid returns to its original color.

The decolorization methods are specially used in high viscosity or non-Newtonian systems (Paul et al., 2004). These systems often have persistent dead zones which can easily be detected in transparent tanks by visual methods. In these systems, if measurement probes are used, they should be placed in appropriate regions, in order to avoid errors. For this purpose primary experiments should be carried out to determine the optimum probe position.

Quantitative mixing time measurements can be carried out by means of several different techniques. The most appropriate method will depend on the fluid specifications and the mixing scenarios.

Off-line sampling consists of the addition of a chemical marker to the fluid such as salt, acid or dye and the subsequent removal of these markers. In each sample the concentration of the marker is measured, and the degree of uniformity is obtained by these measurements. This technique is not appropriate when very short mixing times are involved.

Another method is the measurement of thermocouple-based mixing time. This test can be done by adding a liquid with different temperature from the bulk. The temperature in different points of the tank is monitored over time and the mixing time is inferred by the probe outputs. This technique is appropriate for nonconducting fluids. However, the disadvantage of this method is that it is not applicable where the physical properties of the ingredients are very sensitive to temperature changes.

The conductivity probe mixing time is another technique which is used, primarily with low viscosity fluids (Germain, 1979). This technique makes use of an electrolyte in the added liquid as a marker and the conductivity probe monitors the local conductivity over time; from these measurements the probe calculates the mixing time for the system. This technique is not appropriate for nonconducting systems or for systems in which the rheological properties are sensitive to changes in salt concentration. This technique is cheap and easy to use and the conductivity probe gives the mixing time rapidly even in systems where the mixing time is very short.

2.4 Specific objectives

Many efforts have been made to understand the complex principle mechanisms which govern the solid and liquid phases in suspensions. A large number of these studies have focused on determining the principle parameters which have an influence on the just-suspension impeller speed (N_{js}) in low viscosity fluids. The rheological model of dilute and concentrated suspensions in Newtonian and non-Newtonian mediums also helps in the understanding of these mechanisms.

No studies characterizing the mixing of two phase systems with a high viscosity continuous phase in dual-shaft mixers have been performed. Therefore, we propose the following specific objectives:

- To characterize the power consumption and determine the mixing time for high viscosity continuous phases in dual-shaft mixers.

- To characterize the power consumption for high viscosity solid-liquid dispersions in dual-shaft mixers and determine the dispersion time in order to investigate the homogenization efficiency of dual-shaft mixers for high viscosity solid-liquid dispersions.

Chapter 3 – Methodology

In this chapter the methodology of the experiments is presented. In the first section the experimental setup is explained. In the second section, the materials used in the experiments are specified, and finally the experimental strategy demonstrates how the specific objectives will be satisfied.

3.1 Experimental setup

The experimental setup consists of

- A cylindrical polycarbonate vessel with a torispherical bottom shape and 60 liters volume.
- AC motor, capable rotating a Deflo impeller shaft at a nominal velocity of 3600 rpm.
- AC motor, capable of rotating a Paravisc impeller shaft at a nominal velocity of 1760 rpm.
- A torque sensor having a range of 0-30 N.m (with an accuracy of ± 0.1 % full scale) for the Paravisc impeller.
- A torque sensor having a range of 0-10 N.m (with an accuracy of ± 0.1 % full scale) for the Deflo impeller.
- Two optical tachymeter (with an accuracy of ± 0,1 tpm) to measure the rotational velocity of the impellers.
- A 15:1 velocity reducer reduces the rotational velocity of the Paravisc to about 115 rpm.
- Temperature sensors will be placed on the vessel wall near the Deflo impeller in order to avoid degradation of materials resulting from the high shear produced by this impeller.
- To feed the powder into the tank, a volumetric feeder consisting of a conical hopper and a vibrating channel is used.

The experimental setup used for this study is shown in Figure 3-1.

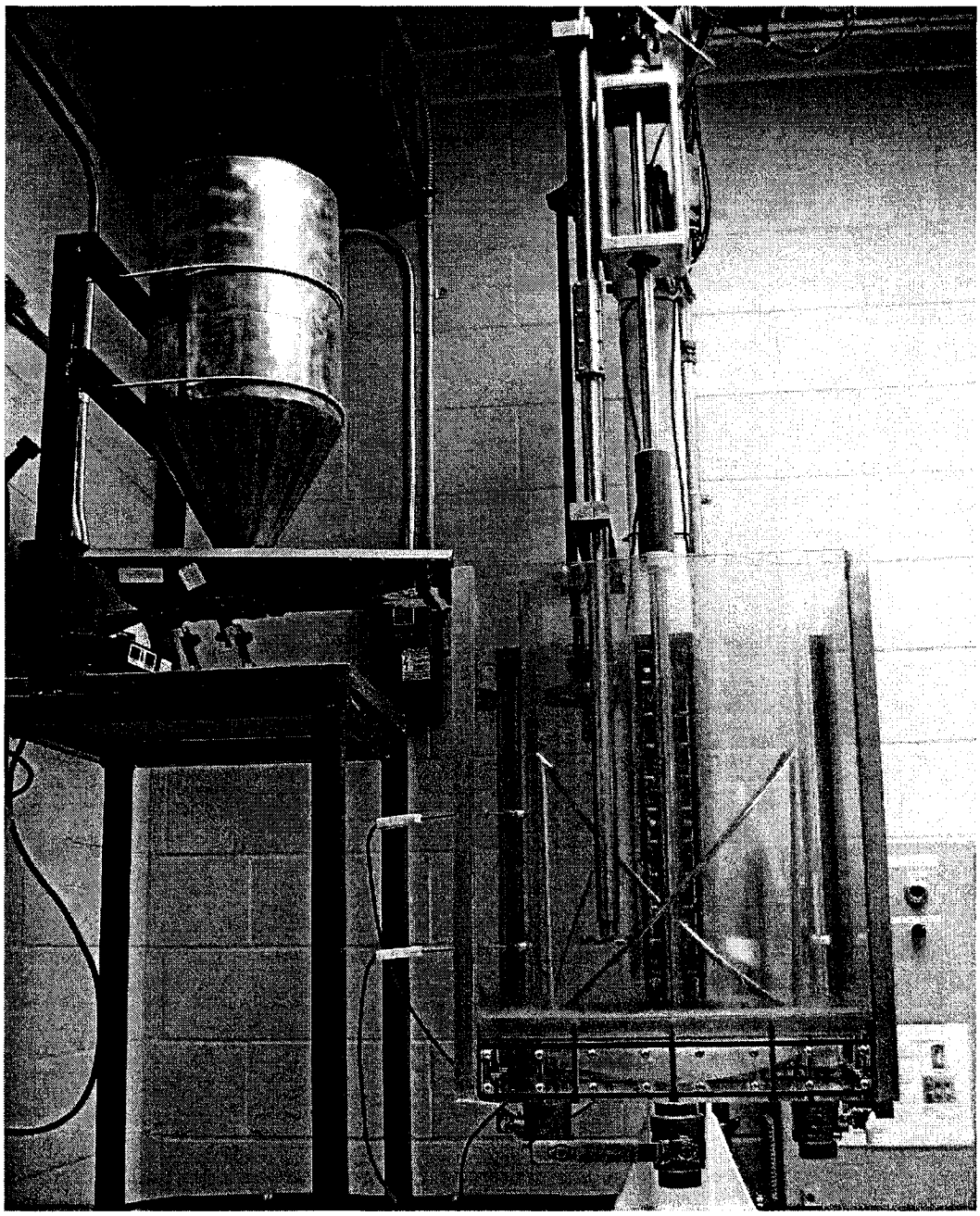

Figure 3-1 Photo of the experimental setup

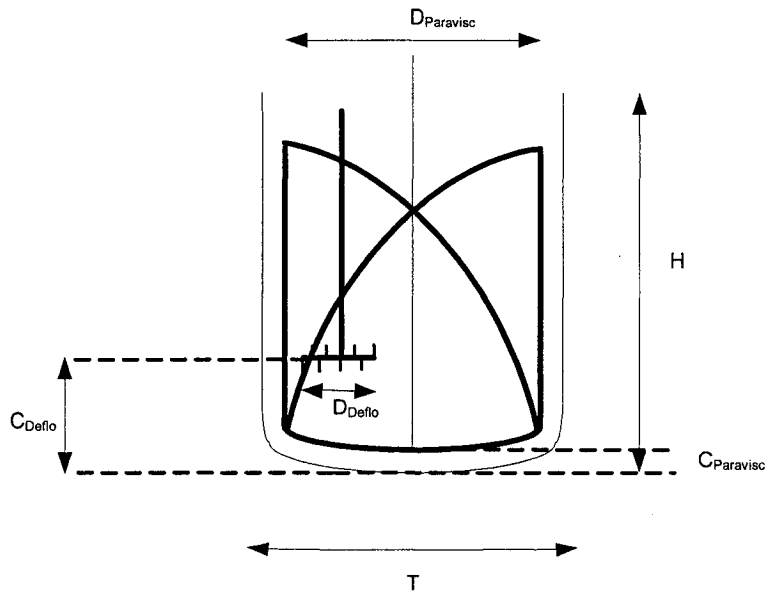

Figure 3-2 Schema of the experimental setup

The laboratory dual-shaft mixer used for this study is shown in Figure 3-1. The vessel and the impeller specifications can be seen in Figure 3-2 and Table 3-1:

Table 3-1 Laboratory dual-shaft mixer parameters

Vessel	Cylindrical polycarbonate vessel torispherical bottom shape Tank diameter (T)	 0.4 m
Distributor	Paravisc (inspired by Ekato) Impeller diameter ($D_{Paravisc}$) Impeller bottom clearance ($C_{Paravisc}$)	 0.374 m < 0.02 m
Disperser	Deflo Impeller diameter (D_{Deflo}) Impeller bottom clearance (C_{Deflo})	 0.08 m $\frac{1}{3}H, \frac{1}{2}H$

The PARAVISC agitator is a low shear agitator that promotes gentle mixing and stimulates lateral and transverse flow. Running at rotational speeds from 0 to 90 rpm, it promotes efficient heat and mass transfer and batch homogeneity (Cohen and Langhorn, 2004). The Paravisc helps to disperse heat within the vessel by stimulating mass flow and continuously removing stagnant material from the tank walls and bottom and pushing it toward the interior. The Paravisc is well adapted to mix high viscosity fluid. In solid-liquid mixing where the homogeneity of the suspension is crucial, and distributing the solid particles into the viscous medium is a difficult task, using the Paravisc has great advantages. Thus, in order to prevent the solid particles from accumulating somewhere in the tank, to provide top-to-bottom flow and increase the suspension homogeneity the Paravisc will be used as a low speed impeller.

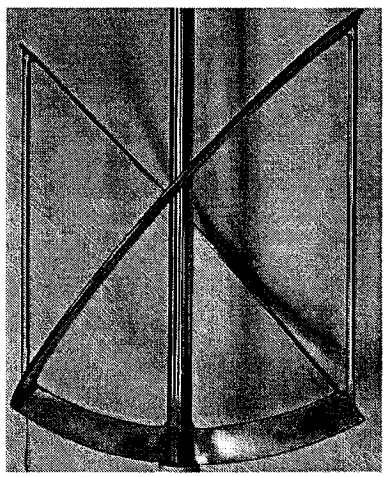

Figure 3-3 Schema of the Paravisc impeller

The Deflo impeller is a high speed disperser which rotates at speeds of up to 1300 rpm (Cohen and Langhorn, 2004). It has the ability to provide high shear and high flow. It is designed to break up any lumps present by causing water to penetrate the interstitial space inside the pigment aggregates where capillary action is the main flow mechanism. It consists of a disc turbine, edged with slightly oblique teeth, alternately angled up and down. This disperser is able to promote good slurry dispersion in highly pigmented solid slurries (as high as 70 wt %) (Furling et al., 2001).

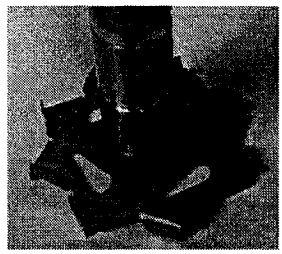

Figure 3-4 Deflo disperser

3.2 Materials

3.2.1 Continuous phase

Glucose-water solutions will be used in the experiments as the Newtonian continuos phase. This type of fluid is transparent with the viscosity varying from 1 to 11 Pa.s and the fluid density varying from 1000 to 1400 Kg/m^3. Because the viscosity of the glucose-water solution is sensitive to temperature changes, process temperature will be measured, allowing us to correct for the viscosity caused by temperature evolution. The rheological properties of the solutions will be determined at different temperatures and different concentrations with a rheometer (AR 2000, TA instruments), using a Couette configuration of 30 mm and 28 mm as the diameter for the inside and outside cylinders. Subsequently, the flow curve (viscosity vs. shear rate) and the viscosity vs. concentration curve at different temperatures will be obtained for each solution.

3.2.2 Solid – liquid system

The solid phases in the experiments will consist of calcium carbonate and glass beads. During the introduction of the pigments, the torque which is applied on the impellers and their rotational speed will be measured. Once the introduction of pigments is completed, the following measurements will be carried out:

- Power consumption evolution with time.

- Particle size distribution of the dispersion, using samples taken with a mastersizer "S" from Malvern .
- The rheological behavior of the dispersion by rheometer.

3.3 Experimental Strategy

Throughout the experiments fundamental knowledge about the mixing power consumption and the degree of homogenization in the dual-shaft mixer as a function of various operating conditions will be obtained. Considering the complexity of the system and the non-Newtonian rheology of the pigment suspensions, it is not practical to address this problem directly.
To do so, we propose the following steps to deal with the complex nature of the problem:

a) Characterization of the power consumption for the Newtonian continuous phase for the following systems:

- Paravisc impeller
- Deflo impeller

b) Characterization of the power consumption for the Newtonian continuous phase at different viscosities in a dual-shaft mixer. The mixing time will be determined using the color-discoloration method. During this stage of the experiment, the influence of different rotational speed ratio on the mixing time and power consumption will be studied.

c) Characterization of the power consumption for solid-liquid dispersions in a dual-shaft mixer. The experiments will be carried out with different viscosities of continuous phase and different solid particle diameters. To verify the mixing efficiency of the dual-shaft

mixer, high viscosity solid-liquid dispersion samples will be taken from the surface of the vessel in order to determine the particle size distribution.

3.3.1 Power consumption

Power consumption will be determined by measuring the torque produced by the impeller rotation. The shaft guiding system induces a residual torque due to friction; hence, the torque value must be corrected by subtracting the residual torque from the measured torque for both impellers:

$$M_c = M_m - M_r \qquad [3\text{-}1]$$

where M_c, M_m and M_r are corrected, measured and residual torques, respectively.

The power dissipated by each impeller in the tank is calculated from the following relation:

$$P = 2 \cdot \pi \cdot N \cdot M_c \qquad [3\text{-}2]$$

where N is the rotational speed of impeller in s^{-1}.

3.3.2 Mixing time

The mixing time has been determined by means of the color-discoloration technique using a fast acid-base reaction, as described by Lamberto et al. (1996). This technique also reveals the possible presence of caverns and dead zones. The mixing time measurements are carried out the following procedure:

- 200 ml of pH indicator solution (0.08 wt% bromo-cresol) is added to the tank
- 10 ml of 10 M NaOH is added and fully mixed until a uniform purple color is obtained

- 50 ml of the purple fluid is taken from the tank and mixed with the 10 ml of 10 M HCL
- This tracer is added to the tank instantly. Hence, the color of the tank changes gradually to the initial yellow color as the mixing proceeds.

The mixing time experiments are recorded on a digital camera (Digital Handycam DCRHC36 MiniDV, Sony). The captured videos are analyzed using the mixing kinetic technique introduced by Cabaret et al., (2006). First, pictures are extracted from the video at different times (minimum of 25 pictures). Then, the pictures are processed by Image analysis using commercial software IMAGE PRO-PLUS 4.5.1 (of Media Cybernetics, USA). This process consists of separating the purple pixels from the yellow pixels (see Cabaret et al., (2006) for details) and plotting an evolution of the number of purple pixels with time. The mixing kinetic is explained by inversion of the obtained evolution. The robustness and reproducibility of the technique was studied by Cabaret al al., (2006). The technique was found to be insensitive to change in light intensity and displayed remarkable reproducibility.

Chapter 4 - Solids dispersion in viscous Newtonian phases using a dual shaft mixer

Sanaz Barar Pour, Louis fradette and Philippe A. Tanguy*

URPEI, Department of Chemical Engineering, Ecole Polytechnique

P.O. Box 6079, station CV, Montreal H3C 3A7, Canada

*Author to whom correspondence should be addressed

Email: philippe.tanguy@polymtl.ca

Submitted to: Chemical Engineering Research and Design (October 2006)

4.1 Abstract

The hydrodynamic performance of a dual shaft mixer consisting of a wall-scraping Paravisc and a high speed Deflo disperser has been experimentally investigated in the case of dispersing fine solids in a viscous Newtonian continuous phase. The experiments were restricted to the laminar regime and made use of two different types of solid particles namely: calcium carbonate and glass beads, at a constant concentration of 10wt. %. Glucose solutions were used as the Newtonian continuous phases. The single phase hydrodynamic characterization showed that the Paravisc power consumption can be significantly affected by the rotation of the Deflo disperser, revealing the good pumping capacity of the turbine. Mixing time measurements showed that the Paravisc effectively controls the bulk flow movement but requires the presence of a baffle, or a second shaft acting as such, in order to output effective mixing performance. This observation is also valid in solids dispersion where the Paravisc impeller exerts a major influence on the time required to achieve a stable dispersion. The homogenization efficiency tests performed showed the ability of the Deflo disperser to efficiently break up the agglomerates in the vessel.

Keywords: dual shaft mixer, solid-liquid dispersion, power consumption, Paravisc impeller, Deflo disperser.

4.2 Introduction

Viscous mixing is involved in many industrial applications like the manufacturing of pastes, putties, chewing gum, soap, and grease (Paul et al., 2004). In these industrial processes, obtaining a uniform mixture is a difficult task, because there are no turbulent eddies to help distribute components. In addition, as most highly viscous solid-liquid dispersions are non-Newtonian, viscous energy dissipation effects occurring during mixing lead to significant temperature variations inside the vessel and induce large viscosity non-uniformity augmenting further the difficulty of the mixing task.

In highly viscous medium, the stresses generated within the liquid are responsible for the breakup and the rupture of agglomerates. To generate those stresses as well as the required bulk flow, a variety of technologies have been proposed such as kneaders, internal mixers, and planetary mixers. All these mixers incorporate high shear zones for dispersion and regions where the fluids are mainly circulated. Another option is the use of multi shaft mixers.

Conceptually, multiple shaft mixers are capable of integrating several mixing functions in one vessel. Typical configurations include a low speed central shaft equipped with a close clearance impeller and a dispersing turbine mounted on a high speed shaft. As they involve separate mixing shafts, from an industrial standpoint, their design, construction, and maintenance are far easier than concentric shaft mixer.

Delaplace et al. (2000) have studied the power consumption and homogenization performance of a particular helical ribbon impeller called Paravisc (Ekato) with an anchor at its bottom. This new impeller is well adapted to highly viscous fluid mixing. It promotes gentle mixing, good pumping, and also helps to remove stagnant material from the tank walls and bottom. The Paravisc prevents the formation of stagnant zones and as the pitch ratio of the Paravisc is higher than that of a helical ribbon, the shear rate induced is higher. A comparison of the performance of the Paravisc and a double helical ribbon impeller also reveals that the pumping capacity of the Paravisc is not improved

by using a higher pitch ratio (Delaplace et al., 2000). However, its power consumption is increased due to the presence of the anchor at the bottom.

High speed impellers are used to generate the high shear forces required to disperse or dissolve a solid phase. The process duty of these impellers is to break the agglomerates and reduce the particle size within the dispersion. This type of impellers must be operated at very high rotational speed which results in very high power consumption. In order to reduce the power consumption, Furling et al. (2001) developed a new impeller technology called Deflo. The Deflo turbine is a modified sawtooth impeller where the number of teeth has been reduced and the teeth orientation permits a better pumping capacity. They characterized the performance of this new impeller in terms of power consumption and mixing quality in a high concentration pigment slurry (70 wt %). The results of their experiments reveal that the Deflo impeller requires less power consumption than a classical Cowles dispersers while the shear level and the pumping capacity provided by Deflo is high enough to incorporate the pigments throughout the vessel and burst the agglomerates.

During the design of a mixer system the major task is to select the most appropriate technology according to the process specifications. The selecting criterion is often based on mixture quality (homogenization) and the power consumption (Holland and Chapman, 1966). In order to predict the performance of a mixing system many studies have focused on the power consumption and the mixing time.

Pahl et al. (1996) have characterized the power consumption of a triple shaft mixer. The mixer was equipped with an anchor impeller, a toothed disc and a propeller. The experimental results show that the power consumption of each impeller decreases in the triple shaft configuration due to the mutual impellers interactions.

Thibault and Tanguy (2002) have studied the power consumption of a new coaxial mixer combining a wall scraping arm on one shaft and a series of wetting rods and a pitched blade turbine on the second shaft, the shafts being operated in a counter-rotating mode. They found that the power was a function of the speed ratio of the fast agitator to the slow agitator in both laminar and turbulent regime.

The literature survey carried out on the unconventional mixing systems has highlighted the lack of scientific knowledge on dual shaft mixers performance. It also highlights the fact that there is a serious problem of defining representative characteristic dimensions. To contribute to a better understanding of this technology, it is proposed to characterize the power consumption and the hydrodynamics of dual shaft mixer equipped with a low speed Paravisc-type helical ribbon impeller and a Deflo disperser. The objective of this work is to evidence the synergy between the two impellers firstly by means of their respective power consumption, and secondly by means of the mixing time and the degree of homogeneity reached during the dispersion of solids.

4.3 Materials and Method

The experimental setup used for this study consists of a cylindrical polycarbonate vessel and torispherical bottom shape of 0.39 m inner diameter and 0.58 m height (Figure 4-1). The liquid height of 0.37 cm was kept constant throughout the tests, so that the total fluid volume was 50 L.

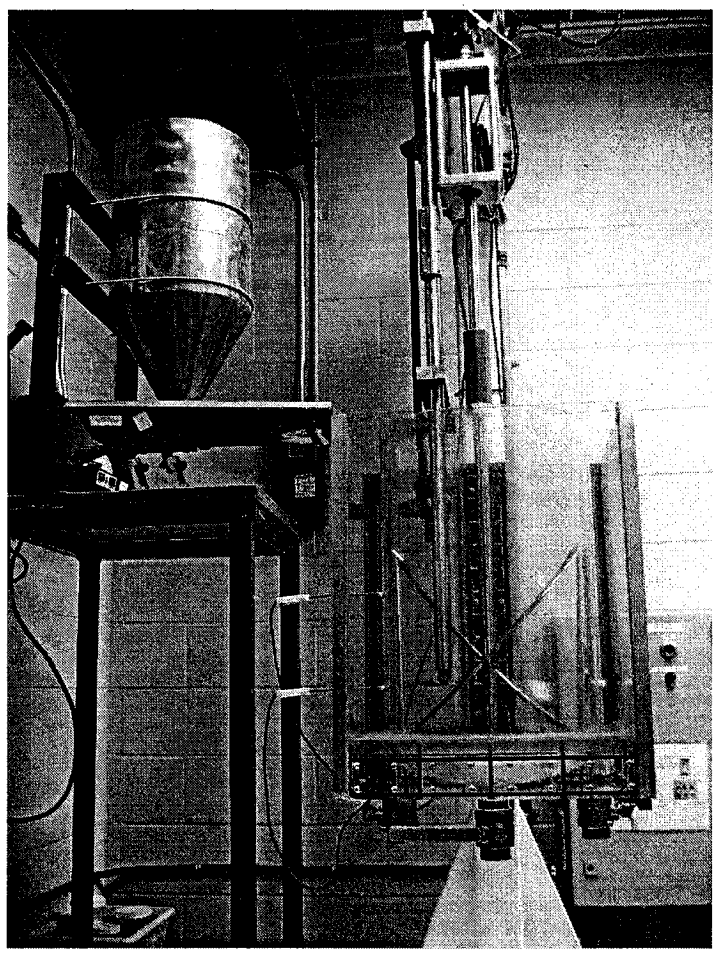

Figure 4-1 Experimental setup showing the mail vessel and the solid feeding system

(a) 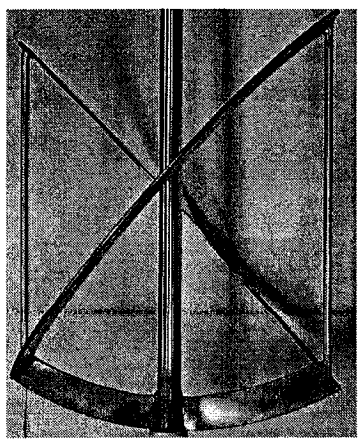 (b) 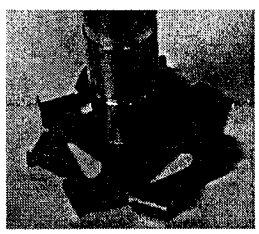

Figure 4-2 Impellers (a) Paravisc (b) Deflo

The dual shaft mixer used in this work consists of two impellers: a centered low-speed low-shear Paravisc-type impeller and an off-centered high-speed high-shear Deflo disperser. Figure 4-2 shows the actual impellers used in this study. The Paravisc-type impeller has a rounded bottom which fits with the torispherical bottom shape of the tank and operates from 0 to 60 rpm. The Deflo impeller is a high speed disperser which rotates from 0 to 1000 rpm. The Deflo disperser is located at 1/4 of the tank diameter and has the ability to be displaced axially. In the experiments, the height of the Deflo was set at 1/3 and 1/2 of the fluid level in single phase and solid-liquid experiments, respectively. Each impeller is equipped with its own speed drive and both shafts operate in co-rotating, clockwise mode.

Aqueous solutions of glucose syrup were chosen as the Newtonian continuous phase. The rheological properties of the solutions were determined at room temperature (~ 23 °C) with a rheometer (AR 2000, TA instrument) by using a Couette configuration of 30 mm and 28 mm diameters for the inside and outside cylinders, respectively. The viscosity of the Newtonian fluids ranged from 1 to 11 Pa.s, and its density between 1350 to 1410 kg/m^3. As the viscosity of the glucose is very sensitive to temperature, two temperature sensors were mounted near the disperser to track the temperature evolution in each experiment. Calcium carbonate and glass beads were used as the dispersed phase with a mean diameter of 3 μm and 140 μm, respectively. The target concentration of the dispersed phase was 10 wt% in all the experiments.

To feed the dispersed phase in the tank, a volumetric feeder consisting of a conical hopper and a vibrating channel was used. The rheological properties of the slurry were determined using the same rheometer as for the liquid phase only. A Mastersizer "S" (Malvern, UK) was used to measure the dispersion particle size distribution. The rate of powder incorporation for calcium carbonate with the volumetric feeder was chosen as 0.51 kg/min. Using the same vibrating frequency, a rate of 0.98 kg/min was obtained for glass beads. Controlling the glass beads incorporation at a lower rate was very difficult and less reproductible. The very weak cohesiveness of the beads explained this

experimental difficulty. Samples were collected always at the same spot from the surface to determine the rheological properties and measuring the dispersion state by means of the particle size distribution.

The power consumption of an agitator is an important factor in any mixer design. Generally, the power consumption of an impeller with Newtonian fluids is expressed in terms of a power number N_p and a Reynolds number Re defined as follows:

$$N_p = \frac{P}{\rho N^3 D^5} \qquad [4\text{-}1]$$

$$\mathrm{Re} = \frac{\rho N D^2}{\mu} \qquad [4\text{-}2]$$

where P represents the power consumption by the impeller, ρ the density of the fluid, N the rotational speed of the impeller, D the diameter of the impeller and μ the Newtonian viscosity.

To determine the power dissipated by the two impellers, the shafts were fitted with two torque meters, which ranges were 0 to 30 N.m for the slow shaft and 0 to 10 N.m for the fast shaft, respectively. The shaft guiding system induces a residual torque due to the friction; hence, the torque value must be corrected by following:

$$M_c = M_m - M_r \qquad [4\text{-}3]$$

where M_c, M_m and M_v are corrected, measured and residual torques, respectively.

The power dissipated by each impeller in the tank was calculated from the following relation:

$$P = 2 \cdot \pi \cdot N \cdot M_c \qquad [4\text{-}4]$$

The LabVIEW software (National Instruments) was used to set and monitor the drive speed and for data acquisition.

The mixing times were evaluated by means of a discoloration method based on a fast acid-base indicator reaction (Fox and Gex, 1956). This technique also reveals the

presence of caverns and dead zones, when present. Approximately 200 ml of pH indicator solution (0.08 wt% purple Bromocresol) is added to the tank to visually differentiate acidic (yellow) and alkaline (red) conditions. At t=0 an acidic injection is made along the shaft at the surface of the liquid. The mixing kinetics curves were generated by an image analysis technique (Cabaret et al., 2006). With this technique each experiment is recorded by a video camera and the captured videos are processed to output mixing kinetics from which the mixing time is easily extracted at a chose value of the % mixing reached.. In this work, 90% mixed state from the mixing kinetics curve was chosen as the mixing time.

4.4 Single phase results

Single impeller.

The characteristic power curve was established for the two agitators individually (Figures 4-3 and 4-4). These results served to estimate the power drawn during the mixing operation and to quantify the eventual interactions between the impellers. We show in Figure 3 that the Paravisc impeller operates in the laminar regime for Re values lower than 100 and for larger values the regime becomes transitional. In Figure 4-4, for the Deflo disperser, the change in power consumption towards the transition regime is rather at Re of 10. Table 4-1 shows the individual K_P value of each impeller in single mode operation.

Table 4-1 Power constant for each impeller

Impeller	K_P
Paravisc	369
Deflo	96

Delaplace et al. (2000) have reported that the K_P value of the Paravisc is equal to 315. The difference between the two K_P values can be explained by the different designs in the Paravisc geometry. The results show the strong effect of the geometry of the impeller on the K_P value.

In the case of the Deflo disperser Foucault et al. (2004) found a K_P value of 65. In the present study the Deflo disperser was located in an off-centered position, near the wall of the vessel, at $T/4$, where T is the diameter of the vessel. The only explanation for such a higher value is that the wall interacts strongly with the Deflo, which in turn increases the power consumption compared to a rotation far from any obstacle as in Foucault's work.

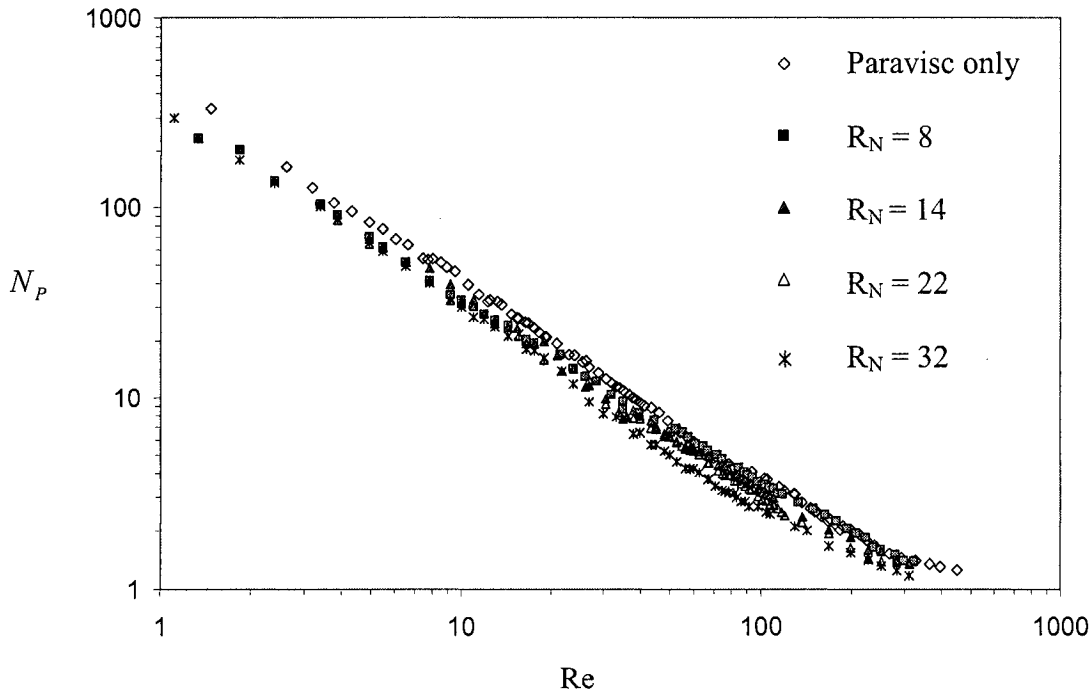

Figure 4-3 Power curve for Paravisc impeller in dual shaft mixer in different rotational speed ratios

Contrary to classical mixing systems, the determination of the power curve of a dual shaft mixer is difficult, as the choice of diameter and speed required to calculate N_P and

Re is unclear. No study is available on the characterization of such a system. Pahl et al., (1996) have characterized the power consumption of a triple shaft mixer by fixing the Reynolds number of one agitator and changing the Reynolds number of the other two agitators gradually. In the present study the influence of the rotational speed ratio ($R_N = N_{Deflo} / N_{Paravisc}$) on the power consumption of the whole system is analyzed. Figure 4-3 shows the characteristic power curve of the Paravisc based on the rotational speed and the diameter of the Paravisc impeller for different rotational speed ratios.

In this figure it can be observed that the Paravisc power draw decreases as the speed ratio increases. It means that for identical Paravisc Reynolds numbers, the power consumption is lower when the speed ratio is higher. In fact the Deflo disperser drags the Paravisc in the flow direction, which lowers the power consumed by the Paravisc. The K_P value of the Paravisc for each rotational speed ratio was determined. Table 4-2 shows a constant decrease in the K_P value with the increase in rotational speed ratio.

Table 4-2 Power constant of the Paravisc in dual shaft mixer

R_N	K_P
0	369
8	336
14	333
22	314
32	291

The power curve of the Deflo disperser is illustrated in Figure 4-4. The power results show that the rotational speed ratio has no measurable effect on the power consumption of the Deflo. As the rotational speed of the Paravisc increases (R_N decreases) the Deflo power curve falls on the same curve than the Deflo working in a single shaft mode. In the transitional regime a noticeable scattering appears, typical of this regime. From

Figure 4-4 it can be concluded that the Paravisc impeller has no effect on the Deflo power consumption.

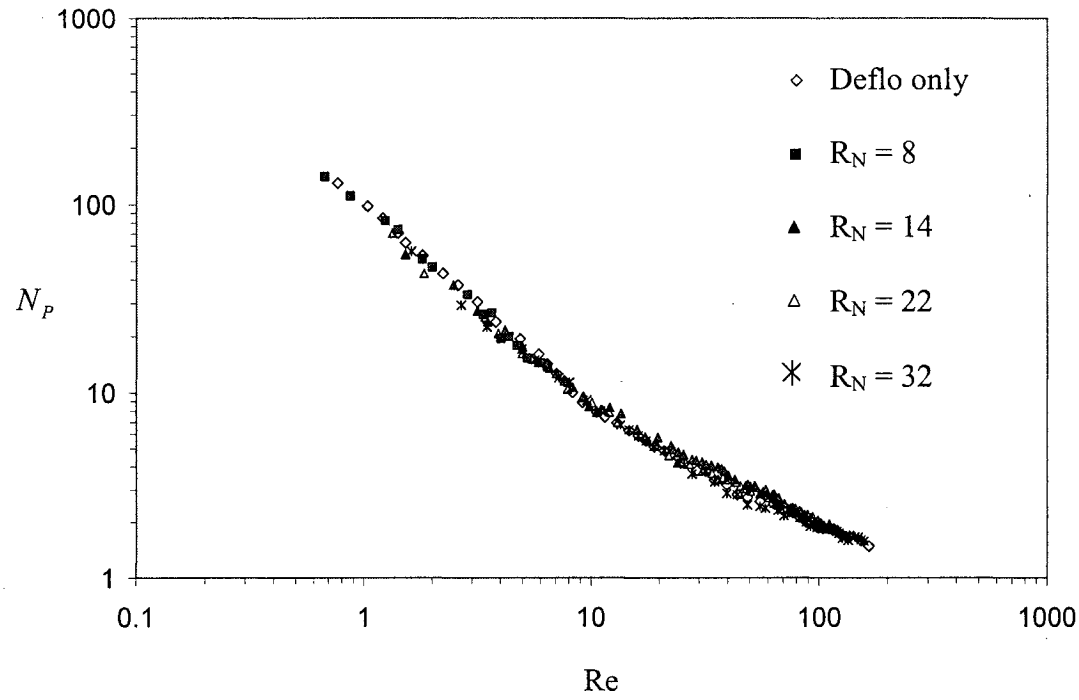

Figure 4-4 Power curve for Deflo disperser in dual shaft mixer in different rotational speed ratios

The mixing time was investigated by considering the range of rotational speeds of the Paravisc namely: 11, 35 and 60 rpm, a rotational speed range of the Deflo from 0 rpm to 1000 rpm with three different continuous phase viscosities. The mixing time with the Paravisc alone where the shaft of Deflo has been removed has also been studied.

The mixing time results show that the Paravisc impeller, when used alone and without the shaft of the Deflo immersed, failed to efficiently mix a considerable volume of the tank and this regardless of the Reynolds number. Figure 4-5 pictures this situation after 20 minutes of mixing. From this figure it is clear that the Paravisc has not mixed the central tank volume and this region remains segregated, which shows the necessity of a

combination of the Paravisc with a baffle of some kind. In this work, the high speed disperser shaft was assimilated to a baffle.

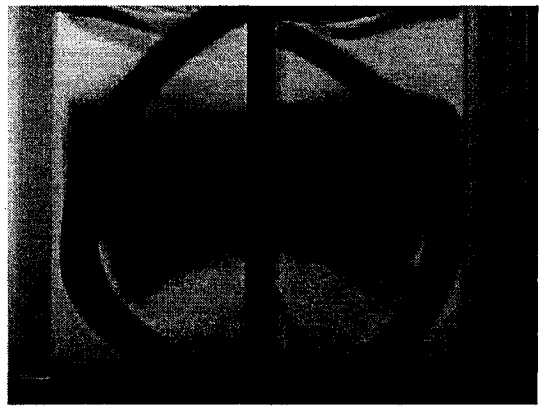

Figure 4-5 Segregated region formed with Paravisc impeller in single shaft mode after 20 minutes at 60 rpm (viscosity = 1 Pa.s)

The mixing time measurements were carried out in order to study the effect of the presence of the Deflo shaft and its rotational speed on the mixing process. Figure 4-6b shows the mixing kinetic curves for a Paravisc rotational speed equal to 11 rpm and for five different rotational speed of Deflo. These curves show that the mixing process is significantly improved by increasing the rotational speed of the Deflo. The Paravisc working alone (single shaft system) is unable to mix 45% of the tank volume, which remains as a segregated region. Increasing the Deflo rotational speed up to 400 rpm has a considerable effect on the mixing time reduction. The kinetics curves show that increasing the Deflo rotational speed further does not lead to such a noticeable increase while the power draw is eight times more.

The mixing kinetic curves obtained for different rotational speeds of the Paravisc for a fixed rotational speed of Deflo disperser (100 rpm) are shown in Figure 4-6a. The discoloration experiments revealed a constant mixing pattern. In the first step, mixing occurs in the region between the Paravisc and the vessel wall. The central bulk region of the tank is the second part that gets mixed. In the last step, mixing occurs on the top

surface and a volume around the central shaft. This figure shows that increasing the rotational speed of the Paravisc from 11 rpm to 35 rpm has considerable effect on mixing time. It also can be noticed that increasing the rotational speed of the Paravisc from 35 rpm to 60 rpm decreases the mixing time to less than 2 minutes; however, the power consumption is three times higher. Figure 4-7 shows the snapshots of the mixing process for a Paravisc rotational of speed 11 rpm with 1000 rpm rotational speed for Deflo and a glucose solution viscosity of 2.3 Pa.s. The snapshots clearly reveal the three step mixing process described above. The pumping action of the Deflo is also evidenced in (b).

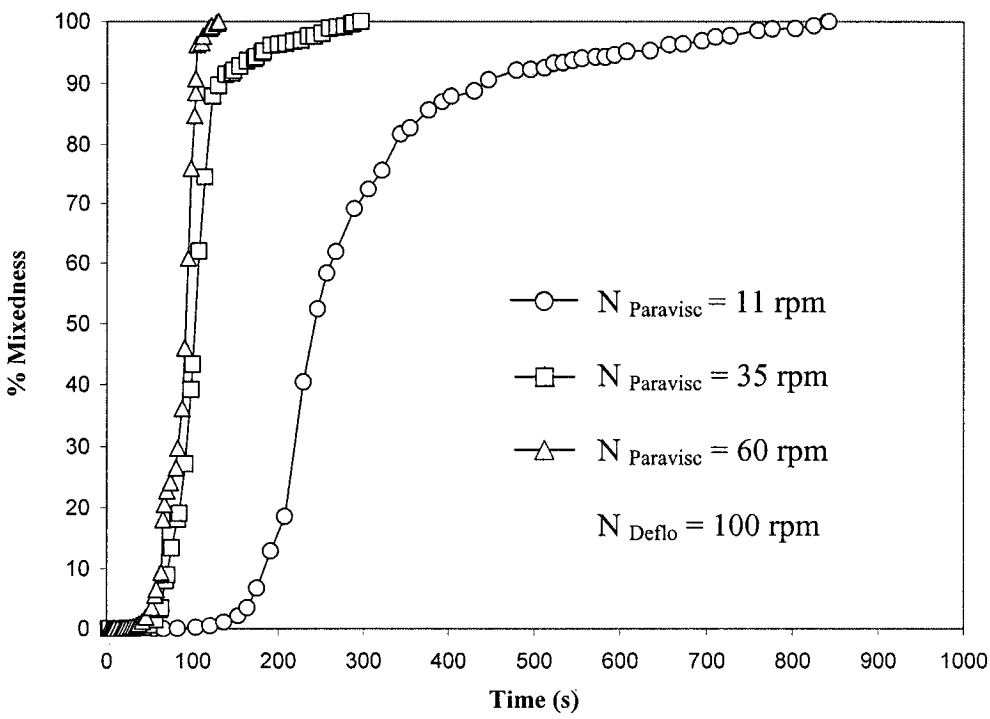

(a)

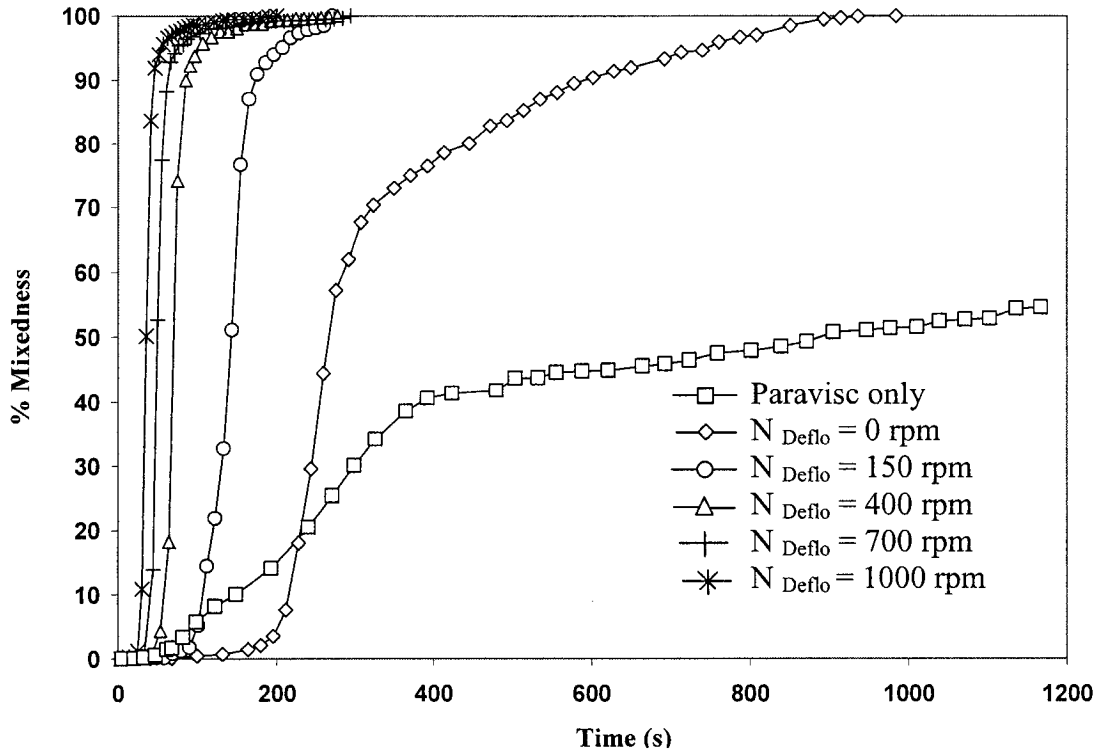

(b)

Figure 4-6 Mixing kinetic curves for Paravisc for Newtonian fluid (a) Influence of rotational speed of Paravisc on mixing kinetics with Deflo at 100 rpm (b) Influence of rotational speed of Deflo on mixing kinetics

Figure 4-8 shows the variation of the mixing time versus the specific power of the mixer. From this figure it can be seen that, as expected, the mixing time decreases with an increase in specific power. However, the influence of the Deflo diminishes with increasing Paravisc rotational speed and viscosity.

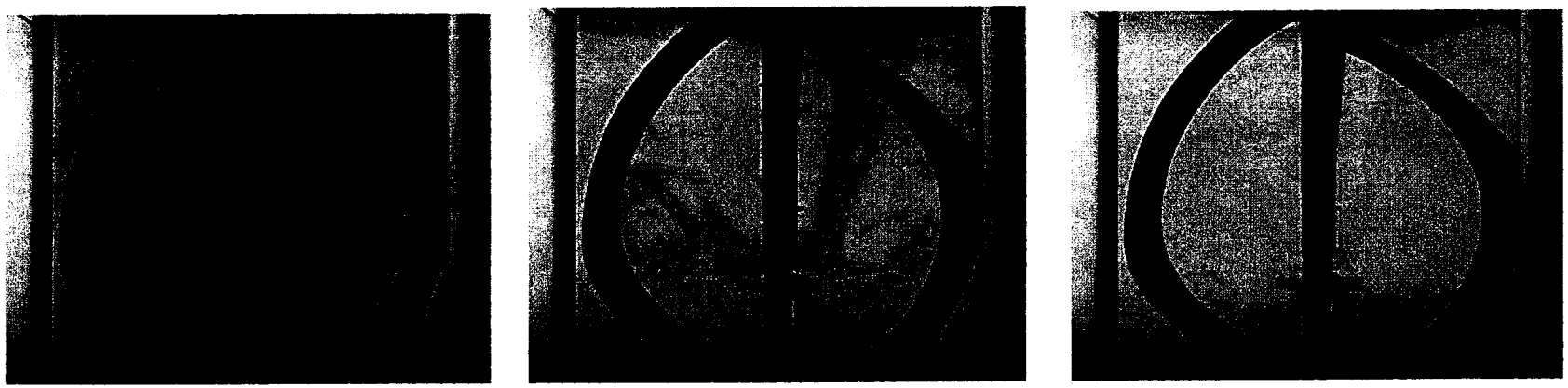

(a) t= 30 s (b) t= 46 s (c) t= 78 s

Figure 4-7 Snapshots of mixing process in vessel, $N_{Paravisc}$ = 11 rpm, N_{Deflo} = 1000 rpm, $\mu_{glucose}$ = 2.3 Pa.s

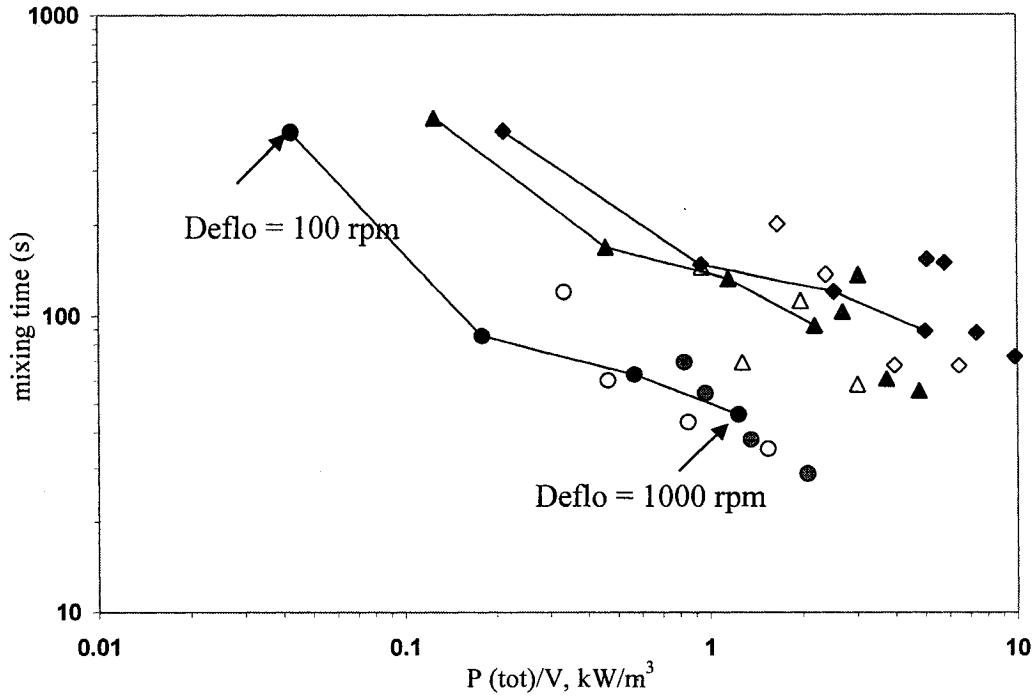

Viscosity, Pa.s	Paravisc speed, rpm		
	11	35	60
2.3	●—	○	●
7.4	▲—	△	▲
10.4	◆—	◇	◆

Figure 4-8 Variation of mixing time versus specific power consumption

In order to better understand the effect of each impeller on mixing, Zlokarnik (2001) proposed to plot the performance of the mixing rate π_3 against the Reynolds mixing time π_2 defined as:

$$\pi_2 = \frac{t\mu}{T^2\rho} \qquad [4\text{-}5]$$

$$\pi_3 = \frac{P_{tot}t^2}{T^3\mu} \qquad [4\text{-}6]$$

where t is mixing time, μ bulk viscosity, T tank diameter, ρ bulk density and P_{tot} the total power consumption of impellers. Figure 4-9 shows the result of the Zlokarnik type analysis. It can be observed that at low viscosity where the Deflo is consuming more that 60% of total power the mixing work is minimum and the Deflo dominates in the mixing process. This figure also indicates that at higher viscosities the optimum mixing performance is obtained when both impellers contribute in the mixing process. The square points in this figure show that during the mixing process the best mixing performance is obtained where power consumption of Paravisc and Deflo impellers is more or less equal (in the 40-60% range of the total power consumption).

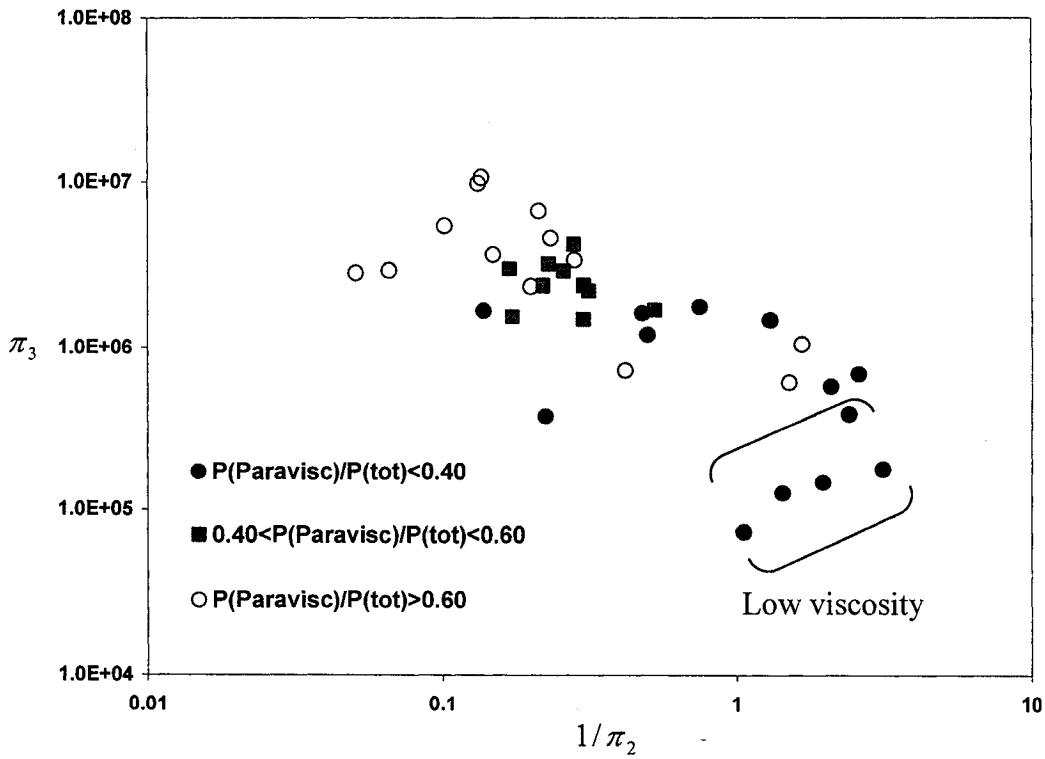

Figure 4-9 Variation of mixing work versus Reynolds mixing time

In this study a new definition was considered for the mixing time analysis. This definition is based on a weighting of the rotational speed of each impeller by their relative power consumption, namely:

$$N' = (N_{Paravisc} \times \frac{P_{Paravisc}}{P_{tot}} + N_{Deflo} \times \frac{P_{Deflo}}{P_{tot}}) \qquad [4\text{-}7]$$

where $N_{Paravisc}$ is the rotational speed of the Paravisc, N_{Deflo} the rotational speed of the Deflo, P_{tot} the total power consumption by the two impeller and $P_{paravisc}$ and P_{Deflo} are the power consumption of the Paravisc and Deflo, respectively.

Figure 4-10 shows the mixing time analysis based on the definition of the dimensionless mixing time vs. Reynolds number. The results show a linear relationship between the

Reynolds number and $N'T_m$, which agrees with the Moo-Young correlation: $N'T_m = a(\mathrm{Re})^b$. Table 4-3 summarizes the coefficients a from the Moo-Young correlation for each viscosity and Paravisc rotational speed. The curves are fitted with an identical slope equal to 0.6. Contrary to the curves generally obtained under the form of the Moo-Young correlation, coefficient b has a positive value. The direct meaning is that increasing the Reynolds number leads to an increase in dimensionless mixing time. What must be kept in mind here is that the increase in Re comes from an increase of the Deflo rotational speed only and that increase in speed is not very efficient at significantly reducing the mixing time. The definition of N′ used also attributes a very important part to the Deflo speed since its power consumption can very often reach 50% and more of the total power consumed on top of which its rotational speed is always an order of magnitude higher than the Paravisc. From the mixing kinetics curves (Figure 4-6 b), it was clearly shown that the Delfo has a significant effect on the mixing time with its major impact solely from its presence in the tank. Further improvements are achieved by the increase in its rotational speed but not as much. We can reasonably say that, with a better pumping impeller (Rushton, propeller, Mixer TT, ...), the dimensionless mixing time vs Re could probably shifted downward or at least reduce the 0.6 exponent observed making this 0.6 value a characterization parameter of the collaboration between the impellers used. This assumption has however to be verified.

The other important observation regards the value of parameter a. Indeed, its value decreases significantly when the rotational speed of the Paravisc impeller is increased. This trend follows along the line of what was presented with the mixing kinetics curves: the Paravisc impeller acts as the most important player in the mixing of the bulk. It must however be remembered that the presence of a baffle (or the presence of a second shaft) is required to reach a good mixing performance (see Figure 4-6b and its related comments).

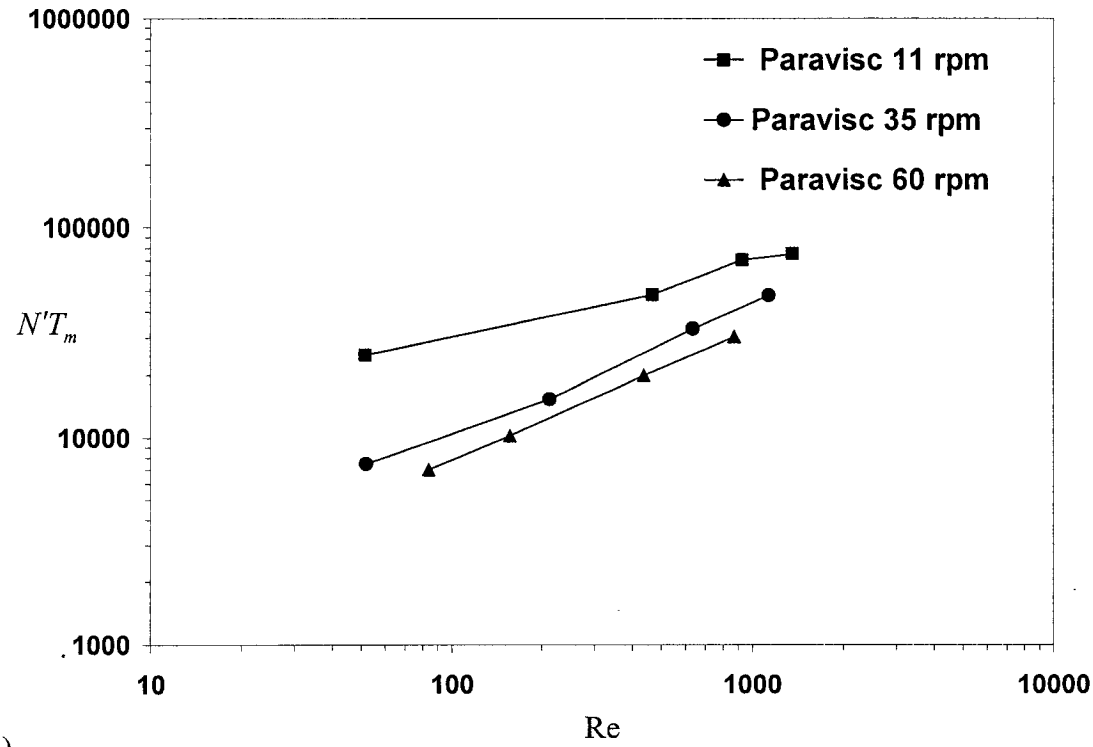
1000000
100000
10000
1000
$N'T_m$
Paravisc 11 rpm
Paravisc 35 rpm
Paravisc 60 rpm
10
100
1000
10000
Re

a)

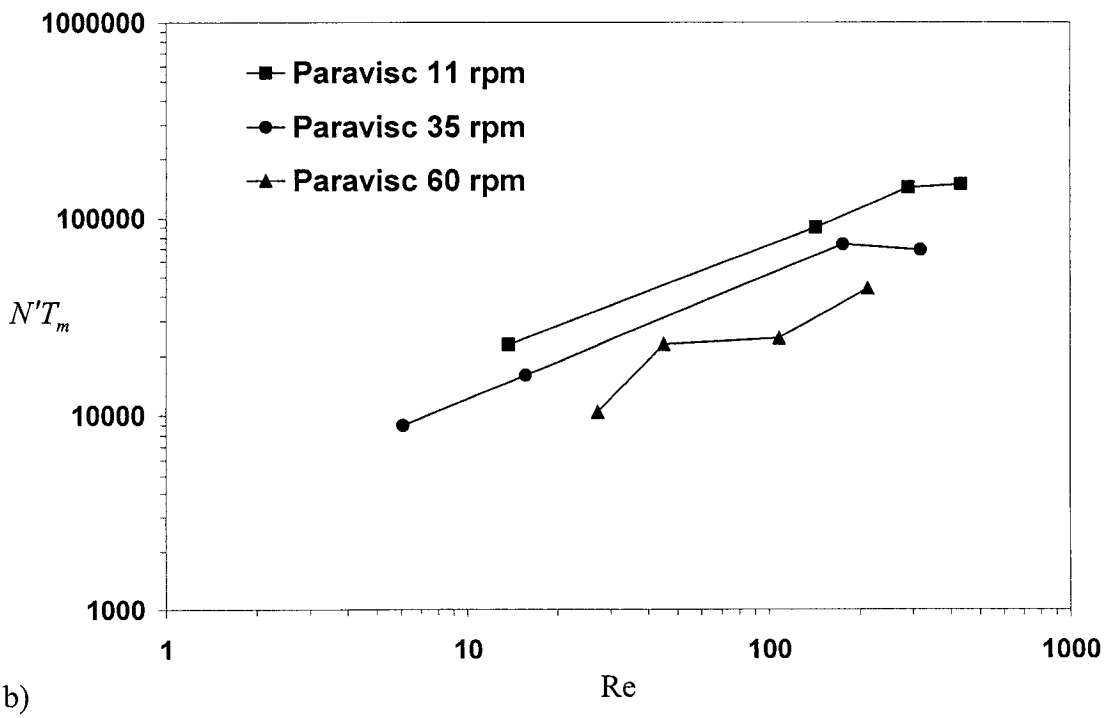
1000000
100000
10000
1000
$N'T_m$
Paravisc 11 rpm
Paravisc 35 rpm
Paravisc 60 rpm
1
10
100
1000
Re

b)

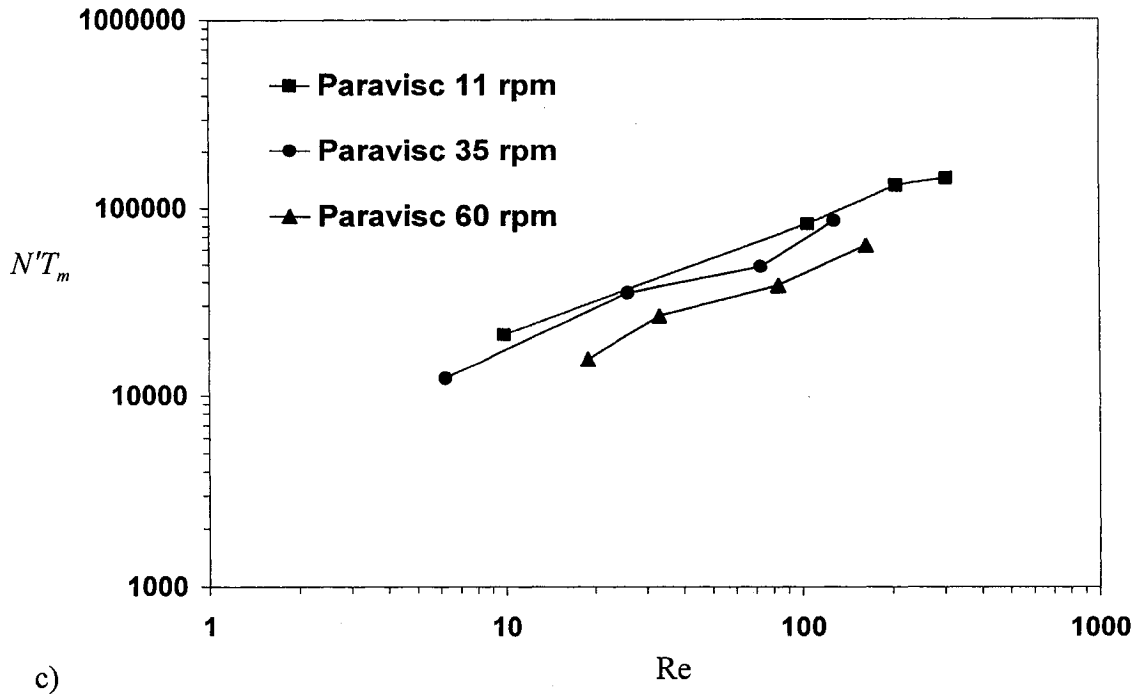

c)

Figure 4-10 Mixing time analysis (a) viscosity 2.3 Pa.s (b) 7.4 Pa.s and (c) 10.4 Pa.s

Table 4-3 Summary of mixing time parameter a ($b = 0.6$)

Viscosity (Pa-s) /$N_{paravisc}$ (RPM)	**2.3**	**7.4**	**10.4**
11	1119	4778	4972
35	691	2545	4312
60	512	1641	2960

4.5 Solid-liquid dispersion

Figure 4-11 shows a general solid-liquid dispersion specific power consumption curve. It was obtained at a speed of 50 rpm for the Paravisc and 500 rpm for the Deflo with a viscosity of 1 Pa.s for the continuous phase. It is representative of all solids addition curves obtained during the experiments. It can be seen that the Paravisc power consumption increases with the solid particle content until a power peak is reached, always a short delay after the addition of the solids in the tank has been completed. The time of the power peak occurrence always matches the end of the dry powder incorporation in the slurry. After this time, the dispersion process continues as manifested by the decrease in torque down to an eventual plateau, where the dispersion is fully achieved as it was described elsewhere (Furling et al., 2001). It can also be seen in Figure 4-11 that the Deflo specific power reaches a minimum after the Paravisc has reached its maximum specific power. This can be explained by the possibility of the formation of the agglomerates in the vessel during the powder feeding due to the highly viscous medium combined to surface effects. As the concentration of the dispersed phase is increasing in the tank, the decrease in the Deflo power consumption is likely due to fluid shear thinning. Once the end of the size reduction process is almost reached, the bulk movement of the fluid tends to equalize the particle concentration in the tank. From this time on, the power consumption increase is caused by an increase in the density and the apparent viscosity of the bulk.

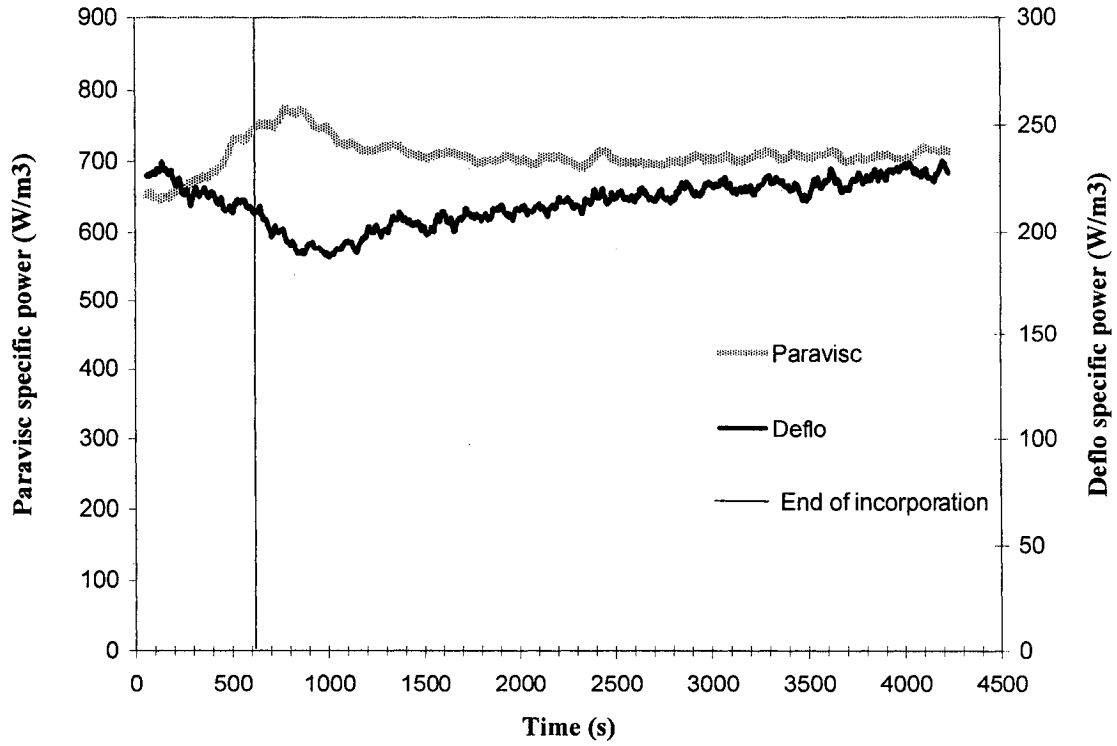

Figure 4-11 General specific power consumption evolution

In order to remove the subjectivity about these phenomena, the particle size of the dispersion was measured at various times during the experiments. Figure 4-12 shows the evolution of the particle size of the calcium carbonate (Paravisc rotational speed = 25 rpm and Deflo rotational speed = 500 rpm). It can be seen that the first sample (Paravis power peak at 950s) contains agglomerates having diameter between 30 μm to 250 μm. However, 1970 seconds the largest particle size of the last sample is only 35 μm. Figure 4-13 shows the effect of the rotational speed of impellers on the particle size of the calcium carbonate. In this figure the particle size of the first sample taken in each experiment is presented. The first sample was taken at the time when no particles remain on the surface of the vessel. As the rotational speed of Deflo disperser increases from 500 rpm to 1000 rpm, the shear forces induced by this impeller are high enough to break up the agglomerates. For identical Deflo rotational speeds, the agglomerates are burst as the rotational speed of the Paravisc increases. This is due to an increased bulk

circulation provided by the Paravisc within the vessel hence favoring the suspension passage in the Deflo region.

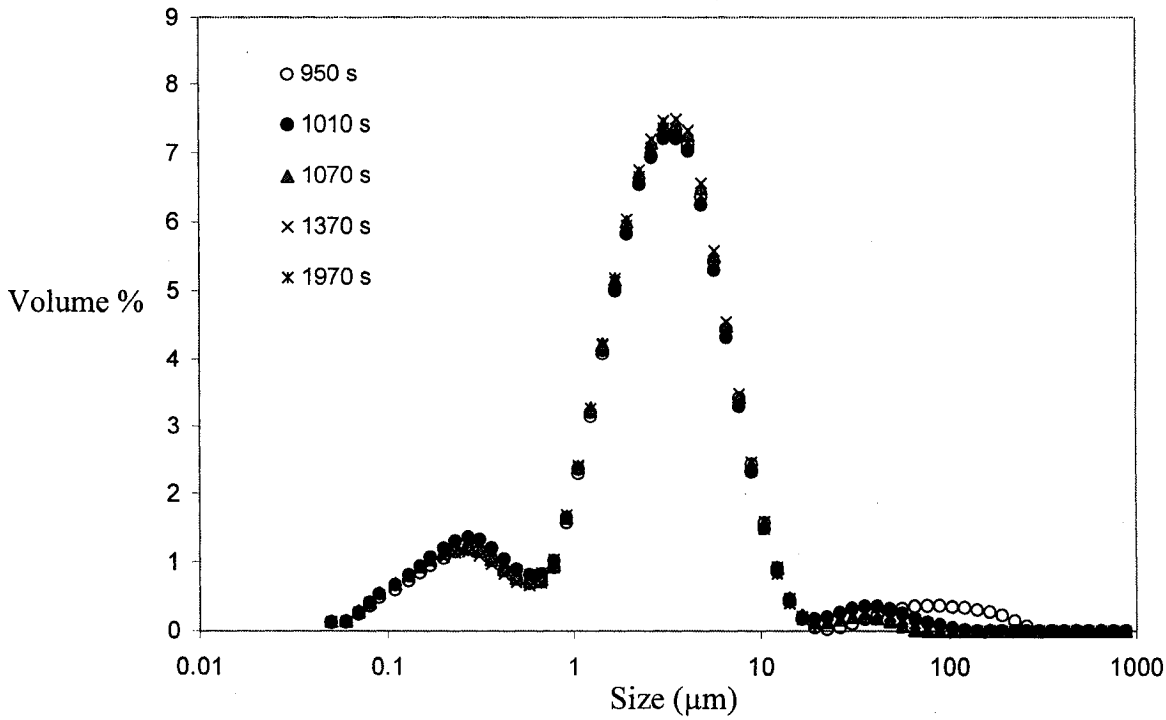

Figure 4-12 Evolution of particle size with time at $N_{Paravisc}$ =25 rpm, N_{Deflo} = 500 rpm

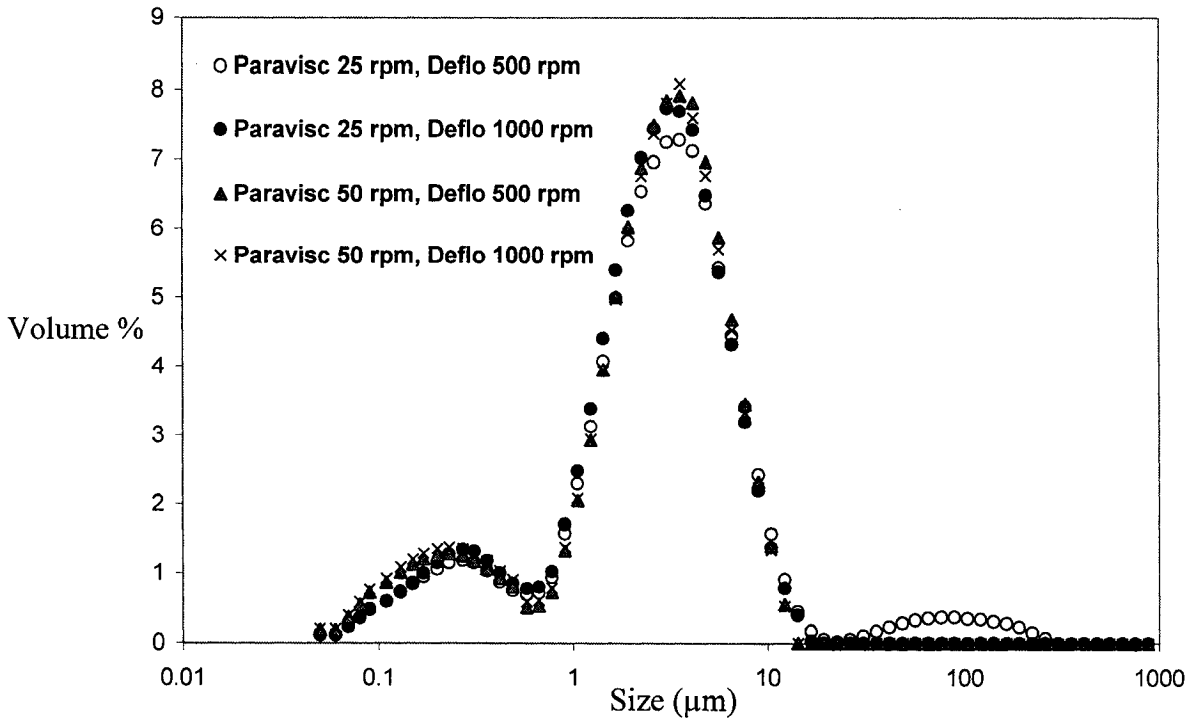

Figure 4-13 Effect of impeller rotational speed on particle size

In order to add to the hypothesis that the Deflo power consumption behavior is due to formation of agglomerates with calcium carbonate, the experiments were conducted using glass beads as the solid particles. Glass beads are known not to form agglomerates. Figure 4-14 shows the influence of the two types of solid particles on the power consumption of each impeller. As expected from apparent density changes, the Paravisc power consumption increases during the addition of the glass beads in the vessel. However, the Paravisc power consumption reaches to a plateau at the end of the incorporation. The power consumption of the Deflo slightly increases for the same reason. The different power consumption behavior observed during the two experiments confirms the assumption of agglomerates formation during the solid-liquid dispersion with calcium carbonate.

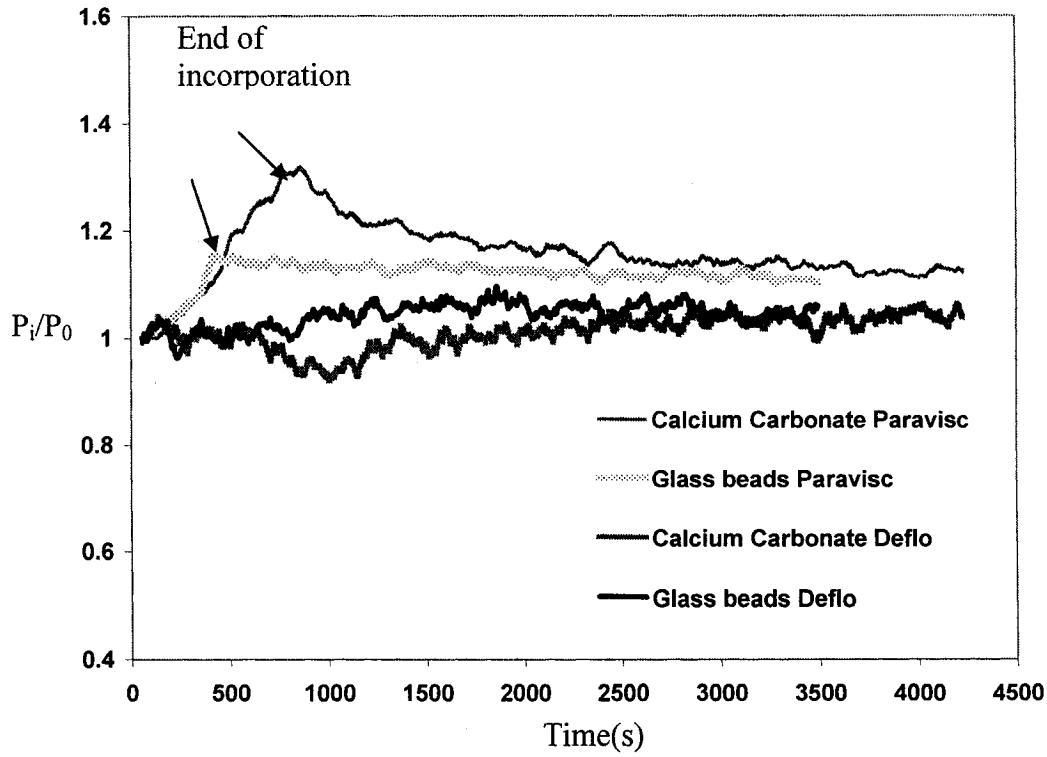

Figure 4-14 Influence of Calcium carbonate and glass beads on impellers power consumption, Paravisc=50 rpm, Deflo=500 rpm

The use of the normalized power draw can be used to identify the effect of the rotational speed of each impeller on the time to reach a stable dispersion state. The normalized values are obtained by reference to the power consumption of each impeller at the start of the experiment when only the continuous phase is present in the tank. Figure 4-15a and 4-15b show the evolution of the normalized impeller power draw for various impellers speeds for the Paravisc and the Deflo, respectively. In figure a it can be seen that as the rotational speed of each impeller increases, less time is needed to reach the plateau. If this is true for both impellers, the effect of the rotational speed of the Paravisc is much more important than the Deflo speed. The trends seen on Figure 4-15b confirm that, as the Deflo rotational speed increase, less time is needed to reach the minimum in the Deflo power consumption.

Figure 4-16 shows the effect of the continuous phase viscosity on the time required to reach a stable dispersion state by means of the normalized power consumption of each impeller. The general behavior of the power consumption for both impellers does not change. The time at which the Paravisc power peak occurs is the same for both viscosities. However, due to the high medium viscosity the onset of power stability for dispersion in case of 11 Pa.s is longer than 1 Pa.s. Mixing times experiments showed the exact same behavior.

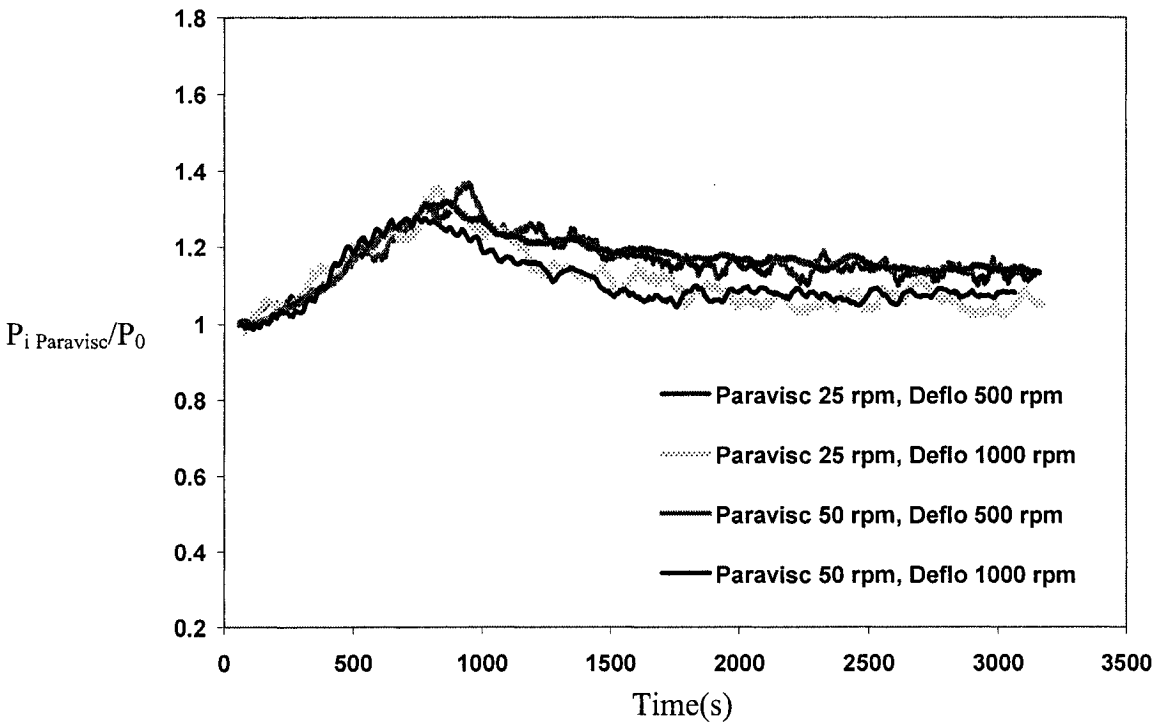

(a)

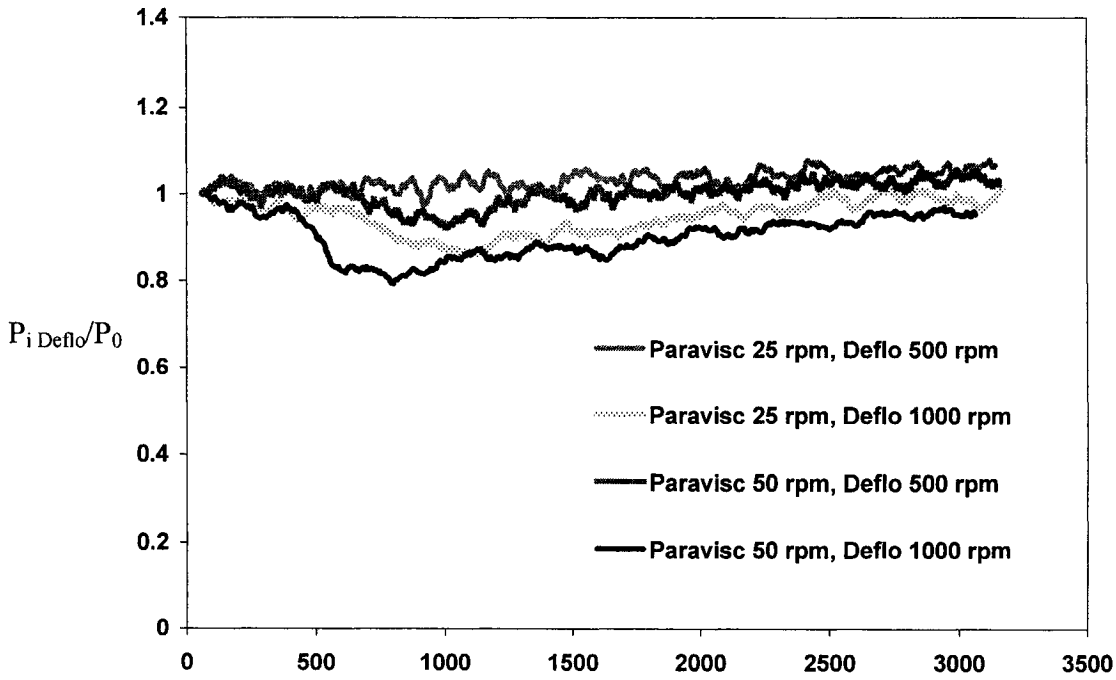

(b)

Figure 4-15 Influence of impellers rotational speed on dispersion

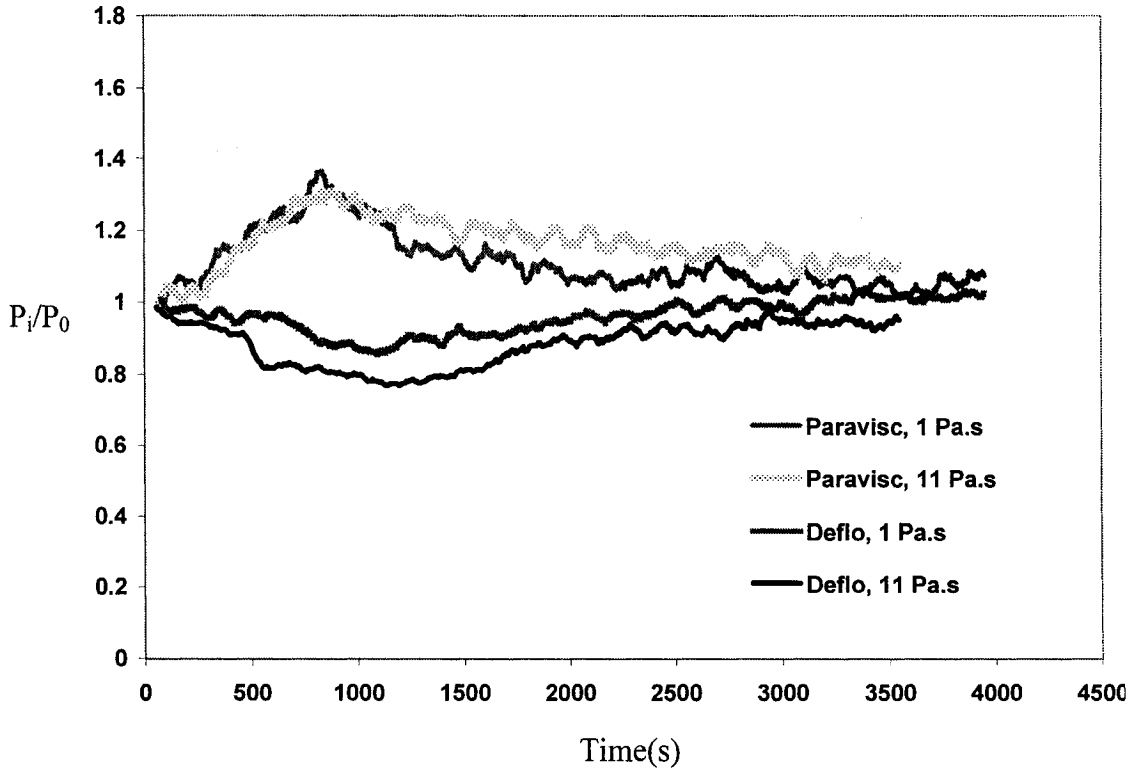

Figure 4-16 Effect of continuous phase viscosity on dispersion Paravisc = 25 rpm, Deflo = 1000 rpm

4.6 Conclusion

The hydrodynamic performance of a dual shaft mixer consisting of a wall-scraping Paravisc and Deflo disperser has been investigated in case of highly viscous continuous phase and solid-liquid dispersion. The experiments showed that increasing the rotational speed of the Deflo lowers the Paravisc power draw. However, the reciprocal was not observed on the Deflo disperser. It was found that the Deflo provides good pumping capacity regardless of the continuous phase viscosity. From the discoloration experiments it was shown that the Paravisc impeller is governing the mixing process,

both in single phase and solid-liquid experiments, but should always work with a baffle (or a high speed impeller acting as such) in order to provide efficient mixing. The power consumption and homogenization efficiency has also been investigated in the case of solid-liquid dispersion. The peak and minimum observed in the power consumption of Paravisc and Deflo was explained by the possibility of formation of particle agglomerates. This hypothesis was validated with experiments using different types of solid particles combined to particle size distributions measurements which also revealed the ability of the Deflo to reduce the particle size and improve the homogeneity of the mixture.

4.7 Acknowledgments

The financial constitution of NSERC and members of the consortium "Innovative Non-Newtonian Mixing Technologies" are gratefully acknowledged. The authors also acknowledge Dr. Avinash Khopkar for his technical contribution.

Nomenclature

Roman Characters

D = impeller diameter, m

$D_{paravisc}$ = Paravisc diameter, m

K_P = power constant

M_c = corrected torque, N-m

M_m = measured torque, N-m

M_r = residual torque, N-m

N' = dual shaft rotational speed, rps

N = impeller rotational speed, rps

N_{Deflo} = Deflo rotational speed, rps

$N_{Paravisc}$ = Paravisc rotational speed, rps

N_P = power number

P = power consumption, W

P_i = power consumption of impeller at second i, W

P_0 = power consumption of impeller at second 0, W

P_{Deflo} = Deflo power consumption, W

$P_{paravisc}$ = Paravisc power consumption, W

P_{tot} = total power consumption, W

Re = Reynolds number

R_N = rotational speed ratio

T = tank diameter, m

T_m = mixing time, s

Greek Characters

ρ = fluid density, kg/m^3

μ = fluid viscosity, Pa.s

θ = dimensionless mixing time

π_2 = Reynolds mixing time

π_3 = Mixing work

4.8 References

Cabaret, F., Fradette, L., Tanguy, P. A.,2006, Characterization of micro mixing kinetics using advance image analysis, Proceedings of 12th European Conference on Mixing, Bologna, Italy, pp 391-398.

Cohen, D., Langhorn, K., 2004, Mix it up, Chemical Processing, 67(4): 31-39.

Delaplace, G., Leuliet, J. C., Gilles, R., 2000, Power requirement when mixing a shear-thickening fluid with a helical ribbon impeller type, Chemical Engineering and Technology, 23(4): 329-336.

Foucault, S., Ascanio, G., Tanguy, P. A., 2005, Power Characteristics in Coaxial Mixing: Newtonian and Non-Newtonian Fluids, Industrial and Engineering Chemistry Research, 44(14): 5036-5043.

Fox, E.A., Gex, V.E., 1956, Single-phase blending of liquids, AIChE Journal, 2(4): 539-544.

Furling, O., Tanguy, P. A., Henric, P., Denoel, D., Choplin, L., 2001, New dispersing turbines for the preparation of concentrated suspensions, Journal of Chemical Engineering of Japan, 34(5): 634-639.

Holland, F.A., Chapman, F. S., 1996, Liquid Mixing and Processing in Stirred Tanks, Reinold Publishing Co.: New York.

Zlokarnik, M., 2001, Stirring; Theory and Practice, Wiley-VCH Verlag GmbH.

Moo-Young, M., Tichar, K., Dullien, F. A. L., 1972, The blending efficiencies of some impellers in batch mixing, AICHE Journal, 18(2): 178-182.

Pahl, M. H., Brenke, A., Luo, Y., 1996, Power Consumption of Multiple Shaft Mixer, Chemical Engineering Technology, 19(6): 503-509.

Paul, E. L., Atiemo-Obeng, V. A., Kresta, A. M., 2004, Handbook of Industrial Mixing, Wiley & Sons.

Thibault, F., Tanguy, P. A., 2002, Power draw analysis of Coaxial Mixer with Newtonian and non-Newtonian fluids in the laminar regime, Chemical Engineering Science, 57(18): 3861-3872.

Chapter 5 - General Discussion

The objective of this study was to analyze the mixing performance of a dual-shaft mixer in highly viscous Newtonian continuous phases and solid-liquid dispersions. This mixer combines a low-speed, close-clearance Paravisc impeller and high speed Deflo disperser which is located in an off-centered position. The impellers are independently controlled and each is powered by an electronic variable speed drive. Despite the widespread industrial use of this type of mixer, no studies have been carried out to characterize the performance of dual-shaft mixer. Experimental investigation of solid-liquid mixing in highly viscous mediums is rare.

The effect of the impellers and the influence of each impeller on the total power consumption were studied. The mixing time measurements showed the effect impellers have on the performance of the mixing process. The results showed that although the Paravisc governs the mixing process, it should always be combined with a baffle or high speed impeller. The Deflo was found to have a great pumping capacity even in highly viscous continuous phases.

The solid-liquid experiments were carried out using highly viscous Newtonian continuous phases. Power consumption measurements and homogenization efficiency were investigated. The Paravisc was found to have a greater influence than the Deflo in achieving a stable dispersion. Particle size distribution measurements were performed showing the ability of the Deflo to break agglomerates in the vessel.

Chapter 6 - Conclusion and recommendations

The hydrodynamic performance of a dual shaft mixer consisting of a wall-scraping Paravisc and Deflo disperser has been investigated in case of highly viscous continuous phase and solid-liquid dispersion. The experiments showed that increasing the rotational speed of the Deflo lowers the Paravisc power draw. It was found that the Deflo provides good pumping capacity regardless of the continuous phase viscosity. From the discoloration experiments it was shown that the Paravisc impeller is governing the mixing process, both in single phase and solid-liquid experiments. The power consumption and homogenization efficiency has also been investigated in the case of solid-liquid dispersion. The peak and minimum observed in the power consumption of Paravisc and Deflo was explained by the possibility of formation of particle agglomerates. This hypothesis was validated with experiments using different types of solid particles combined to particle size distributions measurements which also revealed the ability of the Deflo to reduce the particle size and improve the homogeneity of the mixture.

For future works studying dual-shaft mixers, a few points are recommended:

- The effect of solid phase concentration on solid-liquid dispersion should be studied.
- For high solid concentrations, it would be interesting to study the effect of multiple dispersers on mixing. Locating two dispersers on the high-speed shaft could lead to faster mixing cycles.
- Study the hydrodynamics of dual shaft mixer with different types of disperser in Newtonian and non-Newtonian continuous phases.

References

Ackermann N. L., Shen H. T. (1979). Rheological characteristics of solid-liquid mixtures. AICHE Journal, 25 (2), 327-331.

Alessandrini A., Lapasin R., Sturzi F. (1982). The kinetics of thixotropic behavior in clay / kaolin aqueous suspensions. Chemical Engineering Communication., 17, 13-22.

Armenante P. M., Nagamine E. U. (1998). Effect of low off-bottom impeller clearance on the minimum agitation speed for complete suspension of solids in stirred tanks. Chemical Engineering Science, 53 (9), 1757-1775.

Armenante P. M., Nagamine E. U., Susanto J. (1998). Determination of correlations to predict the minimum agitation speed for complete solid suspension in agitated vessels. Canadian Journal of Chemical Engineering, 76, 413-419.

Armenante P. M., Huang Y., Tong L. (1992). Determination of the minimum agitation speed to attain the just dispersion state in solid-liquid and liquid-liquid reactors provided with multiple impellers. Chemical Engineering Science, 47 (9-11), 2865-2870.

Ascanio G., Brito-Bazan M., Brito-De La Fuente. E., Carreau P. J., Tanguy P. A. (2002). The Canadian Journal of Chemical Engineering, (80), 558-565.

Ayazi Shamlou P., Koutsakos E., (1989). Solids suspension and distribution in liquids under turbulent agitation. 44(3), 529-542.

Barresi A., Baldi G., (1987). Solid dispersion in an agitated vessel. Chemical Engineering Science, 42 (12), 2949-2956.

Baldi G., Conti R., Alaria E. (1978). Complete suspension of particles in mechanically agitated vessels. Chemical Engineering Science, 33, 21-25.

Brunazzi E., Galletti C., Paglianti A., Pintus S. (2004). An impedance probe for the measurements of flow characteristics and mixing properties in stirred slurry and reactors. Trans IChemE, 82(A9), 1250-1257.

Bujalski W., Jaworski Z., Nienow A. W., (2002). CFD study of homogenization with dual Rushton turbines-comparison with experimental results. Trans IChemE, 80, Part A, 97-103.

Chudacek M. W., (1984). Solids suspension behavior in profiled bottom and flat bottom mixing tanks. Chemical Engineering Science , 40 (3), 385-392.

Cohen D., Langhorn K., Charles Ross and Son Co. (April 2004). Chemical Processing magazine, 1-7.

Delaplace G, Leuliet J. C., Ronse G. (2000). Power requirements when mixing a shear-thickening fluid with a Helical Ribbon impeller type. Chemical Engineering Technology 23 (4), 329-336.

Foucault S. (2004) Caracterisation experimental de l'hydrodynamic dans un melangeur coaxial. 143p. Memoire de mitrise es sciences appliquees (Genie Chimique), Ecole Polytechnique de Montreal.

Furling O., Tanguy P.A., Henric P., Denoel D., Choplin L. (2001) Journal of Chemical Engineering of Japan. , 34(5), 634-639.

Gillies R. G., Hill K. B., Mckibben M. J., Shook C. A., (1999). Solids transport by laminar Newtonian flows. Powder technology, 104 (3), 269-277.

Godfrey J. C., Zhu Z. M., Measurement of particle-liquid profiles in agitated tanks. Industrial Mixing Technology. AICHE Symposium Series, 90(299), 181-185.

Gray D. J., Treybal R. E., Barnett S. M., (1982). Mixing of single and two phase systems: Power consumption of impellers. AICHE Journal, 28 (2), 195-199.

Harnby N., Edwards M. F., Nienow A. W., (1985). Mixing in the process industries. Printed and bound in Great Britain by Antony Rowe Ltd, Chippenham, Wiltshire, pp 414.

Jeffrey D. J., Acrivos A., (1976). The Rheological properties of suspensions of rigid particles. AICHE Journal, 22 (3), 417-432.

Jinescu V. V., (1974). The rheology pf suspensions. Int. Chem. Eng., 14(3), 397-420.

Kohler R. H., Estrin J., (?). Power consumption in the agitation solid-liquid suspensions. AICHE Journal , 13 (1), 179-181.

Kraume M. (1992). Mixing times in stirred suspensions. Chemical Engineering Technology , 15, 313-318

Lamberto D. J., Muzzio F. J., Swanson P. D., Tankovich A.L., (1996). Using time-independent RPM to enhance mixing in stirred vessles. Chemical Engineering Science. 51(5), 733-741.

McKee S. L., Williams R.A., Boxman A., (1995). Development of solid-liquid mixing models using tomographic techniques. The Chemical Engineering Journal, 56, 101-107.

Metzner A. B., Otto R. E., (1957). Agitation of non-Newtonian fluids. Chemical Engineering Progress. 3(1), 3-10.

Molerus O., Latzel W. (1987). Suspension of solid particles in agitated vessels-. Archimedes numbers $\leq$ 40. Chemical Engineering Science, 42 (6), 1423-1430.

Molerus O., Latzel W. (1987). Suspension of solid particles in agitated vessels-2. Archimedes numbers $\geq$ 40. Chemical Engineering Science, 42 (6), 1431-1437.

Oldshue J. Y., Herbst N.R., Post T. A. (1990). A guide to fluid mixing. 3 th ed. Lightnin. 153p.

Pahl M. H., Brenke A., Luo Y. (1996). Power consumption of multiple shaft agitators. Chemical Engineering Technology, 19, 503-509.

Pasquali G., Fajner D., (1983). Effect of suspension viscosity on power consumption in the agitation of solid-liquid systems. Chemical Engineering Communication, 22, 371-375.

Paul E. L., Atiemo-Obeng V. A., Kresta A. M., (2004). Handbook of industrial mixing. A John Wiley & Sons, Inc., Publication.

Quemada D. (1978). Rheology of concentrated disperse systems II. A model for non-Newtonian shear viscosity in steady flows. Rheologica Acta. 17, 632-642.

Rieger F., Novak V. (1973). Power consumption of agitators in highly viscous non-Newtonian liquids. Trans. Instn. Chem. Engrs, 51, 1973.

Sessiecq P., Mier P., Cournil M., (1999). Solid particles concentration profiles in an agitated vessel. Trans IChemE, 77 (A), 741-746.

Thibault F., Tanguy P. A., (2002) Power-draw analysis of a coaxial mixer with Newtonian and non-Newtonian fluids in the laminar regime. Chemical Engineering Science, 57, 3861-3872.

Thibault F. (1999) Analalysis du procede de melange solid-liquid : Application a la preparation des sauces de couchage du papier. 252p. These de doctorat en genie chimique. Ecole Polytechnique de Montreal.

Uhl V. W., Gray J. B. (1966). Mixing theory and practice. Volume 1, 2. Academic press Inc. (London) Ltd.

Zwietering TH. N. (1958). Suspension of solid particles in liquid by agitators. Chemical Engineering Science, 8, 244-253.